The reply to the referee report

SciPost-LHCHWG 2025-12-3

We thank the Referee for taking the time to review our manuscript and for the valuable feedback and questions. Below we answer the questions raised by the Referee.

We thank for the suggestions to improve the text for clarity: we have addressed all the typos and comments as explained in details below.

1. *Many abbreviations are used throughout the manuscript without definition. [...]* Thank you for the comment. We now define each abbreviation at its first occurrence in the text.

2. *For a reader not working on this topic, the last diagram in Figure 1 may be confusing since no bottom quarks appear in the final state. [...]* Thank you for the comment, we have extended the caption of Figure 1 in order to make the five-flavour scheme framework clear from the beginning.

3. *On page 3, it is stated that in the 2HDM or the MSSM, $v_{1,2}$ are the vevs of the CP-even Higgs fields. Strictly speaking, this is not accurate [...].* We thank the referee for the comment. We agree that the vacuum expectation values are acquired by the Higgs fields in the gauge basis, as now stated explicitly in the revised draft. Concerning the remark on the CP properties, which we have removed, we note that the Higgs fields in the gauge basis are themselves CP-even. Indeed, the mixing relating gauge and mass eigenstates involves only fields with identical quantum numbers and therefore does not alter their CP properties.

4. *I believe that a word is missing in the last sentence of page 4 [...]* Done, thank you.

5. *A reference to LHAPDF may be in order in section 2. A reference to Pythia 8 should be added when mentioned for the first time in Section 5.1.2 (instead of Section 6.1).* Thank you for pointing it out, we have added the two references.

6. *In Section 2.1, I am somewhat surprised by the use of $\alpha \sim 1/132$ [...]* The value of $\alpha \sim 1/132$ is related to the choice of the G_F-scheme, which is preferred for electroweak corrections in Higgs physics. However, the chosen a value of α is pretty close to the expected on-shell electroweak coupling at the Z-pole. For example, if we consider the hadronic contribution in eq. (10.11) using eq. (10.10) of PDG 2023 (https://pdg.lbl.gov/2023/reviews/rpp2023-rev-standard-model.pdf), we can show that the difference with the input used in our simulation is below 0.7 per cent. In particular, this input is affecting only the overall Yukawa coupling via the determination of the vacuum expectation value, which can be efficiently reweighted. Such difference has the same numerical impact of taking into account complex masses or different renormalisation schemes. In addition, we are not performing EW corrections in the draft, where these choices become relevant.

7. *[...] the authors vary both the scale entering the running of the strong coupling and the scale entering the running of the bottom Yukawa [...]* This recommendation comes from internal studies performed a couple of years ago in the context of MiNNLO$_{PS}$ 5FS predictions. We observed a very small correlation between the renormalisation scale variation of the strong coupling and the Yukawa coupling in this context. The results are obtained in a similar, but not equivalent setup compared to this manuscript (in particular in the 2402.04025 paper): for this reason, we do not quote an explicit numerical impact of the correlated or uncorrelated renormalization scale variation for the two $\overline{\text{MS}}$ couplings. However, these studies showed a really small correlation, with a relative difference below 10% in the determination of the scale variation with or without the correlated variation of the two factors. In particular, we observed that doing a correlated variation of the two scales, which is our current recommendation, makes uncertainty slightly more conservative. In

addition, only in MiNNLO$_{\text{PS}}$ we have disentangled the logarithmic contributions coming from the two renormalisation scales, therefore the correlation of the two renormalisation scale factors is also needed to align the choices of the different implementations.

8. *[...] On page 13, the authors provide a brief discussion of the choice of the jet resolution variable inherent to the Geneva method [...]* Unfortunately, although there exist Geneva implementations that use different resolution variables, they mainly cover different processes. So, for example, the only currently available Geneva implementation for the $b\bar{b} \to H$ process is the one discussed in this report, which uses q_T and a p_T-like version of τ_1. Extending this implementation to different resolution variables requires significant coding work. We plan to make a detailed study of the topic in future work.

9. *On page 14, there is an extra period after the reference to Footnote 4. Furthermore, for completeness, the authors should define the MiNNLOPS damping parameter p explicitly instead of referring the reader to [76]* Thank you, we have explicitly introduced the MiNNLO$_{\text{PS}}$ damping parameter using eq. (5.6).

10. *From the discussion in Section 5.1.2, it appears that cumulant scale choices in Geneva lead to very large uncertainties. If so, it would be helpful to provide a clear recommendation [...]* It is difficult to provide an ultimate recommendation on this topic. Since the difference between the two options is beyond the claimed fixed-order and logarithmic accuracy, there is no "better" or "worse" choice. While the spectrum choice is tailored to predict the distribution of low-p_T events, the cumulant choice is designed to precisely reproduce the results inclusive over the QCD radiation, as explained at the end of section 5.1.1. The two options should then be seen more as additional handles for estimating the theoretical uncertainty of the final predictions, given that they measure the size of a set of subleading contributions.

11. *On page 18, I think that '[...] but deviates from it at higher corrections' should be '[...] but deviates from it at higher orders'. On the same page, the sentence 'Loop effects from SM particles, primarily the top quark, and from SUSY states modify the bottom Yukawa coupling, with these contributions resummed to all orders, which are tan beta-enhanced.' is grammatically unclear and potentially misleading. It should be clarified. Finally, still on the same page, why calling the 5FS the massless scheme?* We have revised the text according to the Referee's suggestions.

12. *A clarification on Eqs. (5.7) and (5.8) would be helpful. Strictly speaking, the single-Higgs production cross section refers to a 125 GeV Higgs. Therefore, the comment on the mass dependence should be moved from Footnote 5 to the main text.* Thank you for the comment. Indeed, we kept implicit that the SM simulation must be performed with the heavy-Higgs mass. We have now moved the relevant component of the Footnote in the text, and we explicitly write the mass of the cross-sections in eq. (5.8).

13. *The numerical values used for the M125 benchmark [...]* The reference we considered is Ref. [115]. We have now refereed to it when we introduce the point in the parameter space we have chosen.

14. *It would be helpful if the authors could comment on the origin of the difference between the NNLO impact on the rapidity distribution shown in Figure 7 and the corresponding result in the SM.* This behavior is related to the high mass of the CP-odd Higgs. The NNLO corrections were more flat in the SM case, in a broader range of rapidity. Due to the heavy Higgs, the distribution is more central with the tails more sensitive to high-order corrections. However, explaining the physical source of this effect is not simple. We believe that this effect is related to the PDF luminosity of the D3-terms of MiNNLO$_{\text{PS}}$. Indeed, due to the high mass of the final state, the convolutions of the luminosity in the MiNNLO$_{\text{PS}}$ formalism receive a bigger numerical impact from the large-x region of the parton distribution functions (evaluated at factorisation scales of order of the transverse momentum of the singlet).

15. *One page 22, the sentence should be better to write [...]* We fixed it, thank you.

16. *I do not understand the reason for using a 9-point scale variation in Section 6.1 [...]* The use of the 9-point scale variation follows the choice adopted in Ref. [23]. We emphasise that the difference between using a 7-point or a 9-point variation is very small in our analysis: the associated scale uncertainty varies by at most 1%

in both the MC@NLO and the MiNNLO$_{\text{PS}}$ simulations. For clarity, we have expanded the corresponding footnote and moved this information into the main text.

17. *On page 29, there is a 'bbH' occurrence that should be written as $b\bar{b}H$ [...]* We have corrected it, thank you.

We hope the answers and the modifications are convincing and the manuscript meets all the requirements for the publication. We remain at your disposal for additional comments.

Best Regards,

Christian Biello and Alessandro Gavardi
on behalf of the authors of the manuscript

Modelling $b\bar{b}H$ production for the LHC at 13.6 TeV

Christian Biello,[a] **Alessandro Gavardi,**[b] **Rebecca von Kuk,**[b] **Matthew A. Lim,**[c,d] **Stefano Manzoni,**[e] **Elena Mazzeo,**[e] **Javier Mazzitelli,**[f] **Aparna Sankar,**[a,g] **Michael Spira,**[f] **Frank J. Tackmann,**[b] **Marius Wiesemann,**[a] **Giulia Zanderighi,**[a,g] **Marco Zaro**[h]

[a] *Max-Planck-Institut für Physik, Boltzmannstrasse 8, 85748 Garching, Germany*

[b] *Deutsches Elektronen-Synchrotron DESY, Notkestr. 85, 22607 Hamburg, Germany*

[c] *Department of Physics and Astronomy, University of Sussex, Sussex House, Brighton, BN1 9RH, UK*

[d] *Università degli Studi di Milano-Bicocca & INFN Sezione di Milano-Bicocca, Piazza della Scienza 3, Milano 20126, Italy*

[e] *CERN, CH-1211 Geneva 23, Switzerland*

[f] *PSI Center for Neutron and Muon Sciences, 5232 Villigen PSI, Switzerland*

[g] *Physik Department T31, James-Franck-Straße 1, Technische Universität München, D-85748 Garching, Germany*

[h] *Università degli Studi di Milano & INFN Sezione di Milano, Via Celoria 16, 20133 Milano, Italy*

Coordinators' e-mail: biello@mpp.mpg.de, marius.wiesemann@mpp.mpg.de

ABSTRACT: We present new state-of-the-art predictions for Standard Model Higgs boson production in association with a bottom-quark pair ($b\bar{b}H$). Updated cross sections are computed in accordance with the recommendations of the LHC Higgs Working Group, including the use of the PDF4LHC21 set of parton distribution functions, with a center-of-mass energy of 13.6 TeV. For the total inclusive cross section, we provide matched predictions of the massless Five-Flavour Scheme and the massive Four-Flavour Scheme at the fixed-order level. We further present recently obtained simulations matched with parton showers in both flavour schemes within the Standard Model, and also discuss them in the context of potential Beyond the Standard Model scenarios. In the massless scheme, we compare different next-to-next-to-leading order predictions matched to parton showers obtained through the MiNNLO$_{PS}$ and GENEVA generators. In addition, the role of Four-Flavour Scheme predictions is studied as a background to HH searches, considering both the top-quark and bottom-quark Yukawa contributions to $b\bar{b}H$ production. Finally, we analyse the sensitivity of the Higgs transverse momentum spectrum to light-quark Yukawa couplings in the diphoton decay channel based on MiNNLO$_{PS}$ simulations.

CDS submission: 9 Sept 2025

LHCHWG approval: 21 Oct 2025

Prepared for submission to SciPost Community Reports.

Contents

1 Introduction

Higgs boson production in association with bottom quarks ($b\bar{b}H$) proceeds via two dominant production mechanisms within the Standard Model (SM). The typically considered $b\bar{b}H$ process proceeds via tree-level diagrams at Leading Order (LO) where the Higgs couples to external bottom quarks, see figure 1 for example, which will be referred to as *Higgs radiation off bottom quarks*. Hence, the cross section is proportional to the squared bottom Yukawa coupling (y_b^2). The other (in the SM even larger) production mechanism is through the *loop-induced gluon fusion process*, where the Higgs couples to the quark loop and a radiated gluon splits into a
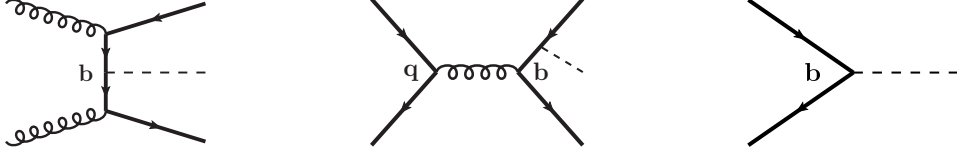
Figure 1: Typical LO Feynman diagrams contributing to $b\bar{b}H$ production in the four-flavour scheme (left, centre) and the five-flavour scheme (right). Incoming particles are shown on the left, and final asymptotic states on the right. In particular, the last diagram represents the LO contribution to the inclusive Higgs-boson production through initial-state bottom-quark fusion mediated by the Yukawa coupling y_b. In the five-flavour scheme, this prediction relies on heavy-quark collinear factorisation: the bottom quark is generated through the PDF evolution, and the description is inclusive with respect to the final state-bottom quark radiation.

bottom-quark pair, see figure 2. The dominant contribution to this process is given by the top-quark loop, and the cross section is therefore proportional to the squared top Yukawa coupling (y_t^2). Interference effects between the two production mechanisms are of order $y_t y_b$, but they are bottom-mass suppressed and appear only if the bottom quark is considered in a massive scheme.

We can thus write the $b\bar{b}H$ production cross section as follows:

$$d\sigma = y_b^2\, \alpha_s^2 \left(\Delta_{y_b^2}^{(0)} + \mathcal{O}(\alpha_s) \right) + y_t y_b\, \alpha_s^3 \left(\Delta_{y_b y_t}^{(0)} + \mathcal{O}(\alpha_s) \right) + y_t^2\, \alpha_s^4 \left(\Delta_{y_t^2}^{(0)} + \mathcal{O}(\alpha_s) \right) , \qquad (1.1)$$

where $\Delta_X^{(0)}$ is the LO contribution to each coupling structure. The first term corresponds to Higgs radiation off bottom quarks, the last term to the loop-induced gluon fusion process, and the central one is their interference. Higher-order corrections, indicated generically by the $\mathcal{O}(\alpha_s)$ (and higher) corrections, are typically computed separately for each process, with the caveat that at higher orders in Quantum Chromodynamics (QCD) the two processes mix, giving rise to their $y_t y_b$ interference contributions. Notice that the loop-induced gluon fusion contribution is formally a Next-to-Next-to-Leading Order (NNLO) correction (relative α_s^2) due to the loop suppression, which however is fully compensated by its y_t^2/y_b^2 enhancement compared to the LO y_b^2 cross section. As a result, the cross section of the y_t^2 contribution is roughly twice as large as the y_b^2 one. There are further relevant $b\bar{b}H$ production mechanisms, including Higgsstrahlung (VH) and Vector Boson Fusion (VBF), but their numerical impact is subleading compared to the y_t^2 and
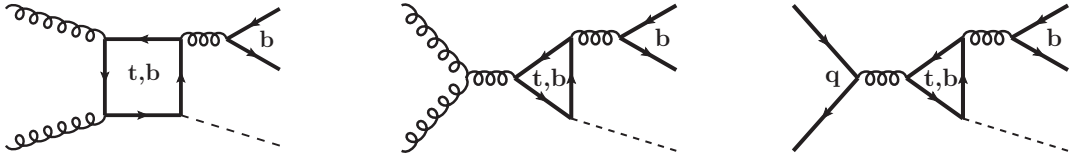
Figure 2: Typical one-loop Feynman diagrams for $b\bar{b}H$ production in the four-flavour scheme. The Higgs boson is produced through radiation off internal heavy-quark loops; for the dominant top-quark contribution, the corresponding vertex is governed by the Yukawa coupling y_t.

y_b^2 contribution, at least for the inclusive cross section. We note that, in experimental analyses, these contributions are already included in the simulations of the VH and VBF processes, and that the corresponding interference terms are negligible.

For fully inclusive Higgs boson production, the radiation off bottom quarks is about two orders of magnitude smaller than the dominant gluon-fusion cross section and ranks at the same size as Higgs production in association with top quarks ($t\bar{t}H$) production. Higgs boson production in association with bottom quarks yields therefore a subleading, but yet relevant contribution to the inclusive Higgs cross section, especially in the precision age of the LHC. However, when b-tagging is applied in experimental analyses, the $b\bar{b}H$ signal yield drops substantially, as the b-jets in this process are typically softer and more forward than those in $t\bar{t}H$ production. In addition, $t\bar{t}H$ events feature a more distinctive event topology with electroweak (EW) signatures, which allows for more effective background suppression. As a result of the small signal yield and involved experimental signature, the measurement of the $b\bar{b}H$ process in the SM has not been achieved yet at the LHC.[1] In the Minimal Supersymmetric Standard Model (MSSM) or the Two-Higgs-Doublet Model (2HDM) of type II, on the other hand, the bottom Yukawa coupling is strongly enhanced for large values of $\tan\beta = v_2/v_1$, where $v_{1,2}$ denote the vacuum expectation values acquired by the gauge-eigenstate Higgs fields, so that this production becomes the dominant one, i.e. even larger than the gluon-fusion mechanism. In addition, $b\bar{b}H$ production is a major background to di-Higgs searches, where at least one of the two Higgs bosons decays to bottom quarks.

The calculation of the $b\bar{b}H$ cross section can be performed in two different schemes. In the Four-Flavour Scheme (4FS), the bottom quarks are massive and thus no bottom Parton Distribution Functions (PDFs) are taken into account so that the bottom quarks are entirely generated in the final state starting from light quark-antiquark and gluon-gluon initial states at LO, see figure 1 (left, center). The calculation requires 4FS PDFs and a 4FS strong coupling α_s in order to avoid artificially large logarithms at higher orders. The 4FS calculation has been performed at Next-to-Leading Order (NLO) QCD some time ago [2, 3], while NNLO QCD results became available only very recently [4].

In the 4FS, the integration over the transverse momenta of the final-state bottom quarks, however, generates logarithmic contributions in the bottom-quark mass that might reduce the perturbative convergence. In order to resum these logarithms, bottom-quark densities need to be introduced by treating the bottom quark as a massless particle. The Dokshitzer–Gribov–Lipatov–Altarelli–Parisi (DGLAP) evolution of the PDFs leads to the resummation. This framework defines the Five-Flavour Scheme (5FS) and starts from a $b\bar{b}$ initial state at LO, see figure 1 (right), which neglects the off-shellness and transverse momenta of the initial-state bottom quarks as well as all power corrections in the bottom-quark mass. The first two approximations are resolved by adding higher-order QCD corrections that, order by order, restore the full kinematics of the bottom quarks. However, finite bottom-mass effects cannot be studied in the 5FS, but they can be included through a combination with the 4FS calculation. The NLO QCD cross section in the 5FS has been obtained some time ago [5, 6]. The NNLO QCD corrections

---

[1]Although no evidence for an observation of $b\bar{b}H$ production has been reported so far, dedicated searches have been performed; see, for example, ref. [1].

[7] can range up to several 10% (depending on the scale settings) and they stabilise the scale dependence significantly. More recently, the 5FS calculation has even been extended to Next-to-Next-to-Next-to-Leading Order (N³LO) QCD [8], which induces a small correction and further reduces the scale uncertainties.

At sufficiently high perturbative order, the two schemes need to approach each other. However, the comparison of the 4FS at NLO and the 5FS at NNLO shows a discrepancy at the level of 20–30%, so that a combination of both schemes became mandatory for reliable prediction. In order to cope with the logarithmic terms in the 4FS, a factorization scale smaller than the Higgs mass has been introduced (typically $M_H/4$) that reduces the differences between the 4FS and 5FS [9, 10]. The combination of the 4FS and 5FS was first performed by applying the empirical Santander matching [11], which is based on a logarithmic weighting between the 4FS and 5FS. This heuristic approach has been replaced by two proper matching procedures some years ago, the FONLL approach [12, 13] and the NLO+NNLL$_{\text{part}}$+$y_b y_t$ method [14, 15]. Both approaches rely on a systematic expansion of the 4FS parameters and 5FS PDFs using different methods to merge the two schemes without double-counting of common contributions. The combined results show a better agreement with the 5FS at NNLO QCD than with the 4FS at NLO QCD. This situation has changed recently with the computation of the NNLO QCD corrections in the 4FS [4]. At NNLO QCD, 4FS and 5FS predictions agree within 10% or better, thus solving the previous discrepancies between the schemes.

Apart from fixed-order predictions, there has been substantial progress also in the matching of NNLO QCD corrections with parton showers (NNLO+PS) for $b\bar{b}H$ production recently. A NNLO+PS calculation in the 5FS has been performed using the GENEVA method [16], while in the MiNNLO$_{\text{PS}}$ framework [4, 17] NNLO+PS predictions for both the 4FS and 5FS predictions have been achieved. These three implementations provide suitable NNLO event generators for the experimental analyses.

The y_t^2-induced contributions to the inclusive $b\bar{b}H$ cross section (cf. figure 2) are not well-defined in the 5FS, since, formally, the rate diverges for massless bottom quarks in fixed-order perturbation theory. Only by selecting bottom-flavoured jets (b-jets), with an appropriate definition of the jet flavour (and imposing kinematical selections on them) fixed-order predictions for the y_t^2 contribution in the 5FS are infrared safe. So far, the size of the y_t^2 contribution to the $b\bar{b}H$ final state has been estimated effectively only at LO in the 5FS, using the inclusive NNLO+PS generator for gluon fusion [18–20]. In this case, reshuffling of the bottom momenta onto the mass shell and matching to the parton shower, where the bottom quarks are considered as massive particles, renders the selection of bottom quarks in the final state finite, even if the underlying perturbative calculation is performed in the 5FS.

In the 4FS, on the other hand, the y_t^2 part of the inclusive $b\bar{b}H$ cross section is finite by construction, since the bottom quarks are treated as massive. On top of that, there is the additional $y_t y_b$ interference contribution in the 4FS, which vanishes in the 5FS.[2] The complete NLO QCD corrections to the top-Yukawa induced terms (both y_t^2 and $y_b y_t$ interference) have been obtained in the Heavy-Top Limit (HTL) [22] and turn out to be substantial. This calculation

---

[2]Throughout this contribution, we consider 5FS to correspond to the massless treatment of all power corrections with $m_b = 0$. Alternatively, the 5FS can be considered to be the leading-power contribution in the bottom-quark mass, thereby including the dominant interference term of $\mathcal{O}(y_b y_t m_b)$, as done in ref. [21] for instance.

has later been extended in ref. [23] to include the parton-shower matching at NLO (NLO+PS) to study $b\bar{b}H$ production as a background to di-Higgs searches. The $y_t\,y_b$ interference amounts to about 10% [2, 3] compared to the inclusive y_b^2 cross section, while the y_t^2 contribution is roughly twice as large as the y_b^2 one [22]. This reduces the sensitivity of the $b\bar{b}H$ process to the bottom Yukawa coupling substantially in the SM. For heavy Higgs bosons in Beyond the Standard Model (BSM) scenarios with an enhanced bottom-Yukawa coupling, however, the radiation off bottom quarks is the dominant contribution, while all top-quark Yukawa induced ones become subleading.

Finally, while the discussion up to here focused on QCD corrections, it is worth mentioning that EW corrections for $b\bar{b}H$ production have also been computed in the 4FS. In particular, they have been first evaluated for the sole gg-induced mechanism [24], and then computed for the full production process [25], and they turn out to be rather small (at the few-percent level). In the latter case, complete-NLO corrections (including QCD and EW corrections) have been computed. In this study, it was also shown that other production mechanisms, specifically VH and VBF, can have a relevant contribution to the $b\bar{b}H$ rate when requiring b-jets, although their impact can be minimised through suitable kinematical requirements, as shown in ref. [26]. Nevertheless, these are additional *backgrounds* to the y_b^2 *signal*, further reducing the sensitivity to the bottom Yukawa coupling in $b\bar{b}H$ final states at the LHC.

In this contribution, we present updated cross section predictions for Higgs boson production in association with bottom quarks in both the 4FS and the 5FS for the y_b^2 contribution and including the $y_b\,y_t$ interference. To provide a consistent overview of state-of-the-art $b\bar{b}H$ predictions at 13.6 TeV centre-of-mass energy, all results are obtained using a common computational setup detailed in section 2. Updated inclusive cross section predictions at 13.6 TeV are reported in section 3, which are obtained by an interpolation of existing LHC Higgs Working Group (LHCHWG) data [27] of the matched NLO 4FS and NNLO 5FS predictions from the NLO+NNLL$_{\rm part}$+y_by_t calculation at 13 and 14 TeV. In section 4, we present the resummed Higgs transverse momentum spectrum in the 5FS at Next-to-Next-to-Next-to Leading Logarithmic (N^{3}LL) accuracy for the y_b^2 component. Section 5 discusses recent developments of Monte Carlo (MC) event generators for the y_b^2 contribution and compares NNLO+PS results from MiNNLO$_{\rm PS}$ and Geneva in the 5FS, consideres MiNNLO$_{\rm PS}$ predictions for heavy Higgs bosons in BSM scenarios, and subsequently examines NNLO+PS predictions from MiNNLO$_{\rm PS}$ in the 4FS. In section 6, we analyse the role of $b\bar{b}H$ production as a background in di-Higgs searches, focusing on both y_b^2 and y_t^2 contributions in phase-space regions relevant for HH studies.

Finally, we discuss a natural extension of the massless calculation for $b\bar{b} \to H$ to describe Higgs-boson production via lighter-parton fusion ($q\bar{q} \to H$). Although these modes are strongly suppressed by the small Yukawa coupling—proportional to the light-quark masses—they receive a PDF enhancement, with distinctive differential effects. We therefore present novel results for Higgs boson production via light-quark fusion at N^{3}LL' + approximate Next-to-Next-to-Next-to-Leading Order (aN^{3}LO) and NNLO+PS in section 7, with particular emphasis on the sensitivity of the transverse momentum distribution on the light-quark Yukawa couplings. We summarise our findings and discuss possible future directions for improved $b\bar{b}H$ predictions in section 8.

2 Computational setup

All simulations in this paper are obtained at a centre-of-mass energy of $\sqrt{s} = 13.6$ TeV, employing the PDF4LHC21_40 (LHAPDF ID 93100) set for the parton distribution functions for massless-scheme calculations and the set PDF4LHC21_40_nf4 (LHAPDF ID 93500) for simulations with massive bottom quarks [28]. We used the LHAPDF interface [29] to utilise the PDF sets in our calculations.

2.1 Numerical Inputs

The parametric inputs, including the strong coupling and EW parameters relevant for the Higgs vacuum expectation value, follow the latest recommendations from the LHCHWG [30] and the Particle Data Group (PDG) parameters [31]. For completeness, the most relevant inputs for $b\bar{b}H$ predictions are reported in the following: The predictions in the massive schemes are obtained using an on-shell value of the bottom-quark mass of $m_b^{\rm OS} = (4.92 \pm 0.13)$ GeV for internal and external bottom quark lines. The Yukawa coupling, on the other hand, is renormalised in the $\overline{\rm MS}$ scheme using an input value of $m_b(m_b) = (4.18 \pm 0.03)$ GeV for the renormalization group running of the Yukawa mass. This scheme choice for the Yukawa coupling is crucial in order to evaluate it at its natural scale, which is of the order of the Higgs boson mass, and to avoid large logarithmic corrections. The scale settings are discussed in the following subsection. The following EW input parameters are used: $m_W = 80.379$ GeV, $\Gamma_W = 2.085$ GeV, $m_Z = 91.1876$ GeV, $\Gamma_Z = 2.4952$ GeV. Employing complex masses with the electromagnetic coupling set to $\alpha = 1/132.3489045$, the corresponding vacuum expectation value is $v = (246.403 - 3.8060\,i)$ GeV. The Higgs boson is considered to be stable in all simulations, except where its decay into photons or tau leptons is explicitly considered. Also in these cases it is treated as on-shell and with zero width. The strong coupling is set to $\alpha_s(m_Z) = 0.1180$ in the 5FS calculations. The corresponding 4FS value is obtained by accounting for heavy-quark decoupling effects, as discussed below. The strong coupling is obtained directly from the corresponding PDF set for consistency.

2.2 Running of the bottom Yukawa coupling

The Yukawa coupling is renormalized in the $\overline{\rm MS}$ scheme in both the 4FS and the 5FS, adapting the following recommendation: We derive the coupling $y_b(\mu_{\rm R}) = m_b(\mu_{\rm R})/v$ by evolving $\hat{m}_b \equiv m_b(m_b) = 4.18$ GeV to $m_b(\mu_{\rm R})$ via four-loop running, solving the Renormalization Group Equation (RGE) [32, 33]. This evolution is directly related to the one of the strong coupling, which is evaluated both at $\mu_{\rm R}$ and at $\hat{m}_b$. In the massless scheme, these values are straightforwardly obtained by evolving the input $\alpha_s(m_Z) = 0.1180$ with four-loop QCD running and $n_f = 5$ active flavours. In the massive scheme, the procedure follows the approach commonly adopted in modern PDF evolution libraries: starting from $\alpha_s(m_Z) = 0.1180$ we evolve down to $\hat{m}_b$ with $n_f = 5$, where the decoupling relation [34] is applied to extract $\alpha_s(\hat{m}_b)$ in the 4FS. This value is then used as a boundary condition to evolve to $\alpha_s(\mu_{\rm R})$ with $n_f = 4$ active flavours.

For consistency, scale uncertainties are obtained by varying the scale with respect to the central one using the order of the evolution consistent with the calculation, i.e. two-loop running

for NLO predictions and three-loop running for NNLO calculations, and with the number of active flavours consistent with the flavour scheme under consideration.

Predictions involving the top-quark Yukawa contribution employ the on-shell definition of the coupling. A top-quark mass of 172.5 GeV is used throughout the simulations.

2.3 Scale settings

A scale choice of the order of the Higgs-boson mass is recommended for the factorization (μ_{F}) and renormalization (μ_{R}) scales. The precise choices of these scales are specified in this Report before the corresponding predictions are presented. The theory uncertainty is estimated using the standard 7-point variation, i.e. by changing the scales by a factor of 2 with the constraint $\frac{1}{2} \leq \mu_{\mathrm{R}}/\mu_{\mathrm{F}} \leq 2$ in order to avoid large logarithmic effects. The renormalization scales associated with the Yukawa coupling and the strong coupling are simultaneously rescaled by the same factor. We have performed detailed studies on the impact of this correlation and found that such a correlated variation provides a reliable estimate of the overall renormalization uncertainty.

In earlier 4FS predictions, a dynamical scale—specifically, one quarter of the transverse mass of the $b\bar{b}H$ system—was often adopted for the Yukawa coupling [35]. Such small scale resulted in higher 4FS cross sections, which reduced the gap with the 5FS predictions. However, with the inclusion of NNLO QCD corrections in the 4FS, such a scale choice is no longer necessary. Moreover, as shown in ref. [4], comparisons between dynamical and fixed scales at NNLO show minimal differences. Consequently, we recommend aligning the scale choices of the Yukawa coupling in the 4FS and 5FS at NNLO QCD accuracy, with a scale of the order of the Higgs-boson mass providing a natural and consistent choice.

3 Updated inclusive cross sections at 13.6 TeV

In this section, we report predictions for the inclusive $b\bar{b}H$ cross section at 13.6 TeV. The best description of the $b\bar{b}H$ process is obtained by combining the calculations in the massless and massive schemes. The 5FS computation includes the resummation of large collinear logarithmic contributions, while the 4FS captures all mass effects order by order in perturbative QCD. As already mentioned in the introduction, two main approaches exist that have been applied to obtain the $b\bar{b}H$ cross section at high accuracy: FONLL [12, 13, 36] and NLO+NNLL$_{\mathrm{part}}$+$y_b y_t$ [14, 15].

FONLL-B [12, 13] and NLO+NNLL$_{\mathrm{part}}$+$y_b y_t$ [14, 15] match the NNLO 5FS and the NLO 4FS cross section. Both approaches yield results that are fully consistent with each other, as shown in ref. [27]. The novel FONLL-C matching [36] adds the N^{3}LO corrections in the 5FS to FONLL-B. The NLO+NNLL$_{\mathrm{part}}$+$y_b y_t$ combination introduces a resummation scale μ_{B}, which enables an estimate of the matching uncertainties. The $y_b y_t$ contribution is easily included as a fixed-order non-singular term, since these interference effects are power corrections that vanish to all perturbative orders in the small bottom-quark mass limit.

The setup of the calculation follows that is described in section 2, with the choice of the following central scales,

$$\mu_{\mathrm{F}} = \frac{1}{4}(m_H + 2m_b), \qquad \mu_{\mathrm{R}} = \frac{1}{2}m_H \,, \tag{3.1}$$

in order to ensure a good perturbative convergence in the fully-inclusive calculation.

In table 1, we report the results of the NLO+NNLL$_{\text{part}}$+$y_b y_t$ combination via a linear interpolation between the existing 13 TeV and 14 TeV results, using the relation

$$\sigma(13.6\,\text{TeV}) = 0.4\sigma(13.0\,\text{TeV}) + 0.6\sigma(14.0\,\text{TeV}) . \tag{3.2}$$

The cross section is provided together with an overall theoretical uncertainty. This includes the standard 7-point renormalization and factorization scale variation, the resummation scale uncertainty, and the uncertainties associated with the PDFs and the strong coupling. An alternative cross section estimation is presented in table 2 where the same numbers have been combined using a logarithmic interpolation. In order to test the accuracy of the interpolation, we have also considered linear interpolation of 13.5 TeV and 14 TeV results. Using the latter, we have estimated the cross section in table 3 with the following linear interpolation,

$$\sigma(13.6\,\text{TeV}) = 0.8\sigma(13.5\,\text{TeV}) + 0.2\sigma(14.0\,\text{TeV}) . \tag{3.3}$$

We observe a good agreement between the cross section values obtained with different interpolations or different choices of boundary conditions. Due to the good accuracy of the interpolation and the substantial theoretical and parametric uncertainty, dedicated runs at 13.6 TeV are not required.

4 Transverse momentum resummation at third order

The Higgs transverse momentum spectrum provides a promising approach for extracting the Yukawa coupling from Higgs boson production processes, because its shape is sensitive to the precise value of the coupling. In particular, one can exploit the pattern of QCD emissions from the incoming quarks and gluons to discriminate between the gluon and various quark channels in the initial state [37]. That is, the radiation pattern for different initial states yields different shapes for the transverse momentum (q_T) spectrum of the recoiling Higgs boson. As a result, a precise measurement of the Higgs q_T spectrum, especially at small q_T, allows one to gain sensitivity to the quark Yukawa couplings [38, 39]. At small $q_T \ll m_H$, this requires the

m_h[GeV]	σ[fb]	$\Delta_{(\mu_R,\mu_F)\oplus\mu_B}$[%]	$\Delta_{\text{PDF}\oplus\alpha_s}$[%]
125.00	569.1	± 8.63	$+3.35/-3.44$
125.09	567.9	± 8.63	$+3.36/-3.44$
125.10	567.7	± 8.63	$+3.36/-3.44$
125.20	566.3	± 8.63	$+3.35/-3.44$

Table 1: Total $b\bar{b}H$ cross sections in the SM for a LHC center-of-mass energy of $\sqrt{s} = 13.6$ TeV obtained via linear interpolation of results from 13 TeV and 14 TeV. The results are given with symmetrised uncertainties from the 7-point scale variation combined with the resummation dependency and the parametric uncertainty from PDFs and strong coupling.

m_h[GeV]	σ[fb]	$\Delta_{(\mu_R,\mu_F)\oplus\mu_B}$[%]	$\Delta_{\mathrm{PDF}\oplus\alpha_s}$[%]
125.00	568.1	± 8.64	$+3.35/-3.44$
125.09	566.9	± 8.64	$+3.36/-3.44$
125.10	566.7	± 8.64	$+3.36/-3.45$
125.20	565.3	± 8.64	$+3.35/-3.45$

Table 2: Total $b\bar{b}H$ cross sections in the SM for a LHC center-of-mass energy of $\sqrt{s} = 13.6$ TeV obtained via logarithmic interpolation of results from 13 TeV and 14 TeV.

m_h[GeV]	σ[fb]	$\Delta_{(\mu_R,\mu_F)\oplus\mu_B}$[%]	$\Delta_{\mathrm{PDF}\oplus\alpha_s}$[%]
125.00	567.7	± 8.86	$+3.30/-3.68$
125.09	566.4	± 8.92	$+3.43/-3.51$

Table 3: Total $b\bar{b}H$ cross sections in the SM for a LHC center-of-mass energy of $\sqrt{s} = 13.6$ TeV obtained via linear interpolation of results from 13.5 TeV and 14 TeV.

all-order resummation of logarithms of q_T/m_H that would otherwise spoil the convergence of perturbation theory in this regime.

In this section, we provide recent results for the resummed q_T spectrum for $b\bar{b} \to H$ at N^{3}LL$'$ order matched to fixed NNLO and aN^{3}LO in the 5FS [40].[3] Previously, the spectrum was calculated to Next-to-Next-to-Leading Logarithmic (NNLL) + NNLO accuracy [42] using the Collins–Soper–Sterman (CSS) formalism [43–45]. For this prediction, we use Soft-Collinear Effective Theory (SCET) [46–50] to resum the logarithms of q_T/m_H which is equivalent to a modern formulation of the CSS formalism. We employ the rapidity renormalization group [51] together with the exponential regulator [52] for which the ingredients required for the resummation at N^{3}LL$'$ are known. The singular cross section can be written in a factorised form as

$$\frac{\mathrm{d}\sigma^{\mathrm{sing}}}{\mathrm{d}Y\mathrm{d}^2q_{\mathrm{T}}} = \sum_{a,b} H_{ab}(m_H^2;\mu)[B_a \otimes B_b \otimes S_{ab}](x_a, x_b, q_{\mathrm{T}};\mu)\,, \tag{4.1}$$

where the kinematic quantities $\omega_{a,b}$ and $x_{a,b}$ are given by

$$\omega_a = m_H e^{+Y}, \quad \omega_b = m_H e^{-Y} \quad \text{and} \quad x_{a,b} = \frac{\omega_{a,b}}{E_{cm}}\,, \tag{4.2}$$

with E_{cm} denoting the hadronic center-of-mass energy. The hard function H_{ab} is process dependent and describes physics at the hard scale $\mu \sim m_H$. The beam functions $B_{a,b}$ and the soft function S_{ab} describe collinear and soft radiation at the low scale $\mu \sim q_T$. The term

---

[3]Here, we use the logarithmic counting of ref. [41], where the prime denotes inclusion of higher order boundary terms.
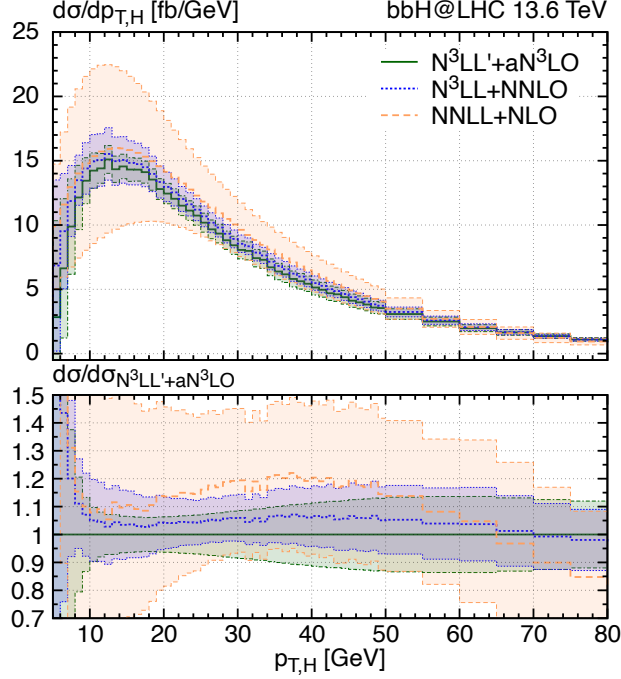
Figure 3: Higgs transverse momentum spectrum in the 5FS predicted by the analytic resummed prediction at NNLO+NLO (orange, dashed), N^3LL+NNLO (blue, dotted) and N^3LL'+aN^3LO (green, solid) accuracy.

$[B_a \otimes B_b \otimes S_{ab}]$,

$$[B_a \otimes B_b \otimes S_{ab}](x_a, x_b, q_T; \mu) \equiv \int d^2 k_a \, d^2 k_b \, d^2 k_s \, \delta^{(2)}(q_T - k_a - k_b - k_s)$$
$$\times B_a(x_a, k_a; \mu, \nu/\omega_a) B_b(x_b, k_b; \mu, \nu/\omega_b) S_{ab}(k_s; \mu, \nu), \qquad (4.3)$$

is usually evaluated in Fourier-conjugate b_T space, as the convolutions in q_T in eq. (4.1) turn into products in b_T space.

To perform the all-order resummation, each function is first evaluated at its own natural boundary scale(s): μ_H, (μ_B, ν_B), and (μ_S, ν_S). By choosing appropriate values for the boundary scales close to their canonical values, each function is free of large logarithms and can therefore be evaluated in fixed-order perturbation theory. Next, all functions are evolved from their respective boundary conditions to a common arbitrary point (μ, ν) by solving their coupled system of RGEs. For more details, we refer to refs. [40, 53, 54]. For the resummation at N^3LL' we require the N^3LO boundary conditions for the hard function [55, 56], and the beam and soft functions [57–61]. We also need the 3-loop noncusp virtuality anomalous dimensions [57, 59, 62–64] and rapidity anomalous dimension [57, 58, 65], as well as the 4-loop cusp anomalous dimension Γ_{cusp} [66–70] and QCD β function [71–74].

To arrive at a consistent prediction, we need to match the N^3LL' resummed cross section to a NNLO Higgs+jet prediction for which we rely on an approximation. Our aN^3LO fixed-order

cross section must contain the correct singular terms which are part of $d\sigma^{\text{sing}}$. Further, there are large cancellations between the singular and the non-singular cross sections at large values of q_T, which must not be spoiled in the approximation procedure. To satisfy both requirements, we developed a general method to decorrelate the singular and non-singular contributions in ref. [40] which involves shifting a correlated piece between the singular and the non-singular [75]. After the decorrelation procedure, we perform a Padé-like approximation for the non-singular $\mathcal{O}\left(\alpha_s^3\right)$ coefficient.

Our numerical results for the resummed and fixed-order singular contributions are obtained with SCETLIB [76]. In figure 3, we show the resummed q_T spectrum for $b\bar{b} \to H$ at different resummation orders up to the highest $N^3LL'+aN^3LO$. The bands show the perturbative uncertainty estimate. For a detailed breakdown of the uncertainties, we refer to ref. [40]. We observe excellent perturbative convergence, with reduced uncertainties at each higher order.

5 Monte Carlo simulations at NNLO+PS

This section highlights recent advancements in MC simulations for modelling the y_b^2 contribution to $b\bar{b}H$ production. The first matching with parton showers was carried out in the 5FS scheme in ref. [17] using the MiNNLO$_{\text{PS}}$ method. More recently, the GENEVA approach has been applied to simulate $b\bar{b} \to H$ production in the 5FS [16]. In this section, we present the numerical comparison of the two matching methods for this process using the LHCHWG-recommended setup detailed in section 2. In the MC simulations with massless bottom quarks, we consider the Higgs mass as the central value for the factorization (μ_{F}) and renormalization (μ_{R}) scales.

We continue by discussing BSM studies using the MiNNLO$_{\text{PS}}$ generator for an example scenario in the MSSM used as a proof-of-concept. The last part of the section is dedicated to the recently developed NNLO+PS MC generator in the 4FS using the MiNNLO$_{\text{PS}}$ method [4], which provides the first calculation of the NNLO QCD corrections in the massive scheme. In this context, we compare MC predictions from the 4FS and 5FS MiNNLO$_{\text{PS}}$ generators.

5.1 NNLO+PS predictions in the 5FS

5.1.1 MiNNLO$_{\text{PS}}$ and GENEVA methods in a nutshell

MiNNLO$_{\text{PS}}$ [77, 78] and GENEVA [79, 80] are two methods that provide a consistent matching between NNLO QCD corrections and parton showers. They both rely on the combination of fixed-order calculations and analytic resummation in the relevant resolution variables to achieve NNLO accuracy. Both have been proven to work with different types of resolution variables [16, 81–83] and they have been successfully applied to obtain NNLO+PS predictions for many processes of colour-singlet production [16, 17, 81, 82, 84–99]. The MiNNLO$_{\text{PS}}$ approach has also been extended and applied to heavy-quark pair production at NNLO+PS [100–102] as well as heavy-quark pair production in association with colour singlets [4, 103]. The two methods follow different philosophies to reach NNLO accuracy, whose fundamentals are presented below.

We start by briefly reviewing the MiNNLO$_{\text{PS}}$ method for colour-singlet production. We refer to refs. [77, 78, 83] for further details. The MiNNLO$_{\text{PS}}$ procedure is derived from the differential matching of the resummation formula in a suitable jet-resolution variable with the fixed-order prediction at NNLO. By choosing a specific matching scheme, where the Sudakov

is factored out, the cross section is cast into a form that has several important features. The structure mimics the one of the parton shower, NNLO accuracy is achieved inclusively over first and second radiation, and due to the Sudakov suppression no slicing cut-off is required, making the procedure very efficient for event generation. The matching to the parton shower is then performed for the second radiation by means of the POWHEG method [104].

In practice, one starts from an NLO+PS POWHEG event generator [105] for colour-singlet F plus one jet J production, which provides the differential description of the second radiation, consistently matched to subsequent emissions by the shower. Such generator includes the NLO FJ cross section (inclusive over the second radiation), which is governed by the following function:

$$\bar{B} = \frac{d\sigma_{\text{FJ}}^{(1)}}{d\Phi_{\text{FJ}}}(\mu) + \frac{d\sigma_{\text{FJ}}^{(2)}}{d\Phi_{\text{FJ}}}(\mu) . \tag{5.1}$$

This formula can now be extended by means of the MiNNLO_PS procedure, which replaces the NLO FJ cross section by the NNLO F cross section with the overall Sudakov form factor in the jet-resolution variable, mimicking the first shower emission.

$$\bar{B} = e^{-\tilde{S}(p_{\text{T}})} \left\{ \frac{d\sigma_{\text{FJ}}^{(1)}}{d\Phi_{\text{FJ}}}(p_{\text{T}}) \left[1 + \tilde{S}^{(1)}(p_{\text{T}}) \right] + \frac{d\sigma_{\text{FJ}}^{(2)}}{d\Phi_{\text{FJ}}}(p_{\text{T}}) + D^{(\geq 3)}(p_{\text{T}}) \, F^{\text{corr}}(\Phi_{\text{FJ}}) \right\} , \tag{5.2}$$

with $e^{-\tilde{S}}$ denoting the Sudakov form factor and the factor F^{corr} spreading the NNLO corrections in the full phase space. Note that it is crucial to choose a jet-resolution variable consistent with the ordering variable in the parton shower in order not to break its logarithmic accuracy. For instance, in the case of standard Leading Logarithmic (LL) transverse momentum ordered showers (which is the current default, and considered throughout here) the transverse momentum of the colour singlet fulfils this criterion. Here, $D^{(\geq 3)}$ contains the relevant terms to reach NNLO accuracy for observables inclusive over first and second radiation. Without these corrections the inclusive observables would only be NLO accurate, as originally introduced in the MiNLO$'$ approach [18, 106].

The original MiNNLO_PS formulation was based on transverse momentum resummation [77, 78], but it can be applied, in principle, to any resolution variable. For instance, it was explicitly derived for N-jettiness in ref. [83], which however formally breaks the LL accuracy of the shower, due to a mismatch of the resummation and the shower ordering variable. Beyond colour-singlet production, the MiNNLO_PS method has been extended to heavy-quark pair production without [100, 101] and with extra colour singlets in the final state [103]. This advancement enables NNLO+PS predictions for $b\bar{b}H$ production not only in the massless scheme, but also in the massive one, allowing for a complete description of bottom-quark kinematics, as discussed in section 5.2.1.

The GENEVA approach also builds on the analytic resummation in jet-resolution variables. The matching in both first and second radiation in GENEVA are achieved through the analytic resummation, opposed to MiNNLO_PS where the second radiation is matched through POWHEG, as discussed before. GENEVA generates the partonic events with the aim of not distorting the spectrum in the zero-jet resolution variable (here generically called r_0). Conceptually, the GENEVA method boils down to three steps.

1. Matching. The r_0 spectrum at fixed order, differential over the phase space with no final state partons Φ_0, is matched additively to its analytic resummation, obtaining

$$\frac{d\sigma}{d\Phi_0\, dr_0} = \frac{d\sigma^{\mathrm{FO}}}{d\Phi_0\, dr_0} + \frac{d\sigma^{\mathrm{res}}}{d\Phi_0\, dr_0} - \frac{d\sigma^{\mathrm{res}}}{d\Phi_0\, dr_0}\Bigg|_{\mathrm{FO}}. \qquad (5.3)$$

The main difference to the MiNNLO$_{\mathrm{PS}}$ matching is that the matching of the resummation is kept in this additive form, instead of factoring out the overall Sudakov form factor $e^{-\tilde{S}}$ in eq. (5.2).

2. Slicing. A slicing scale r_0^{cut} is introduced to separate events where the radiation is not resolved from those where it is, whose distributions are described respectively by

$$\frac{d\sigma_0}{d\Phi_0}(r_0^{\mathrm{cut}}) = \int_0^{r_0^{\mathrm{cut}}} dr_0\, \frac{d\sigma}{d\Phi_0\, dr_0} \quad \text{and} \quad \frac{d\sigma_{\geq 1}}{d\Phi_0\, dr_0} = \frac{d\sigma}{d\Phi_0\, dr_0}\, \theta(r_0 - r_0^{\mathrm{cut}}). \qquad (5.4)$$

This step is not required in the MiNNLO$_{\mathrm{PS}}$ approach, where the exponential suppression by the overall Sudakov form factor makes the differential cross section numerically integrable down to $p_{\mathrm{T}} = 0$ (after regulating the Landau pole).

3. Splitting. The $\mathcal{P}_{0\to 1}$ function is introduced to make the r_0 spectrum differential over the Φ_1 phase space with one final state parton, thus obtaining

$$\frac{d\sigma_{\geq 1}}{d\Phi_1} = \left\{ \frac{d\sigma^{\mathrm{FO}}}{d\Phi_1} + \left[\frac{d\sigma^{\mathrm{res}}}{d\Phi_0\, dr_0} - \frac{d\sigma^{\mathrm{res}}}{d\Phi_0\, dr_0}\Bigg|_{\mathrm{FO}} \right] \mathcal{P}_{0\to 1}(\Phi_1) \right\} \theta(r_0 - r_0^{\mathrm{cut}}). \qquad (5.5)$$

Here, $\mathcal{P}_{0\to 1}$ plays the corresponding role as F^{corr} in eq. (5.2).

The second emission is then generated by iterating this procedure for a one-jet resolution variable r_1 on the $d\sigma_{\geq 1}/d\Phi_1$ differential cross section at NLO. Most GENEVA implementations use the 0- and 1-jettiness $r_0 = \mathcal{T}_0$ and $r_1 = \mathcal{T}_1$ as resolution variables. The first implementation that adopted the colour-singlet transverse momentum $r_0 = q_{\mathrm{T}}$ instead was presented in ref. [81]. This approach was refined and extended in ref. [16] (also using a p_{T}-like observable as 1-jet resolution variable r_1), where the $b\bar{b} \to H$ process was discussed.

A subtlety related to the slicing of the phase space in GENEVA is that, since the scales appearing in the resummed cumulant and spectrum are a function of the resolution variable r_0, the operations of setting the scales and integrating the spectrum do not commute. This leaves us with two main options. Setting the scales in the spectrum (`spectrum` option) provides the best theoretical description of the r_0 distribution in the region of small r_0 at the price of introducing spurious subleading contributions in the distributions inclusive over the radiation. Setting the scales in the cumulant and defining the spectrum as its derivative (`cumulant` option), on the other hand, enforces the generated events to reproduce the exact NNLO inclusive distributions by construction. The numerical difference between the two choices is discussed in the following section, specifically in figure 4.

Besides treating the resolution variables in different ways, the two approaches may also produce small differences in the distributions inclusive over the radiation. The MiNNLO$_{\mathrm{PS}}$ approach can differ from fixed-order NNLO predictions by terms beyond the nominal accuracy,

due to the specific matching scheme, where the Sudakov is factored out. The additive approach adopted by GENEVA, on the other hand, can exactly align terms beyond accuracy with the fixed-order differential NNLO cross section. On the other hand, the presence of the overall Sudakov form factor in MiNNLO$_{PS}$ has the advantage of a better numerical efficiency with a small number of negative weights and without having to deal with large cancellations in a slicing cutoff, as introduced in GENEVA. Distributions sensitive to QCD emissions (which also have lower perturbative accuracy) are instead more heavily dependent on the specifics of the two approaches, and differences between the methods can be used to estimate the respective theoretical uncertainties. Despite these differences, MiNNLO$_{PS}$ and GENEVA are generally agree within their respective uncertainties, especially for observables inclusive over radiation, where any difference is beyond NNLO QCD and should be covered by scale uncertainties.

5.1.2   Numerical comparison of MiNNLO$_{PS}$ and GENEVA predictions

In this section, we present a numerical comparison between two MC generators for $b\bar{b} \to H$ production in the 5FS in the MiNNLO$_{PS}$ and GENEVA frameworks. The settings adopted are described in section 2, with the only notable difference being the treatment of the running bottom-quark Yukawa coupling. The MiNNLO$_{PS}$ predictions follow the setup in section 2 using a four-loop running [32, 33] to evolve the bottom Yukawa from the input to the hard scale, while the GENEVA generator employs a three-loop running throughout derived from SCET. This difference is numerically very small and can be safely neglected in the following comparison. Both the MC generators produce events that are showered using PYTHIA8 [142] with a local recoil.

The MiNNLO$_{PS}$ generator includes an option to change the scale in the resummed logarithmic terms from the scale m_X by a factor of K_Q, where m_X denotes the invariant mass of the final state of the Born process (for $b\bar{b} \to H$, this corresponds to the Higgs-boson mass). This scale $Q = K_Q m_X$ controls the matching of resummed and fixed-order contributions within MiNNLO$_{PS}$[4]. It can be applied to assess the matching uncertainties in the MiNNLO$_{PS}$ generator. The $b\bar{b} \to H$ results are obtained using the default central value of $K_Q = 0.25$, with the alternative choice $K_Q = 0.5$ included in the uncertainty estimate. The overall theoretical uncertainty is assessed via a 14-point scale variation, combining standard renormalization and factorization scale variations with the additional resummation scale variation. In the matching region, the logarithmic contributions are smoothly suppressed towards large transverse momenta using modified logarithms,

$$\ln \frac{Q}{p_T} \to \frac{1}{p} \ln \left(1 + \left(\frac{Q}{p_T} \right)^p \right), \tag{5.6}$$

as originally introduced in ref. [77]. The free positive parameter p is set to the default value, $p = 6$. We have tested alternative parameters for the modified logarithms and found only minor effects, which are well within the MiNNLO$_{PS}$ scale uncertainties.

The GENEVA generator uses the cumulant scale choices in order to have a better agreement of inclusive observables with NNLO QCD predictions. Moreover, it applies default theoretical-uncertainty estimation with the included matching uncertainty as discussed in ref. [16].

---

[4]See section 4.2 of ref. [101] for further details.
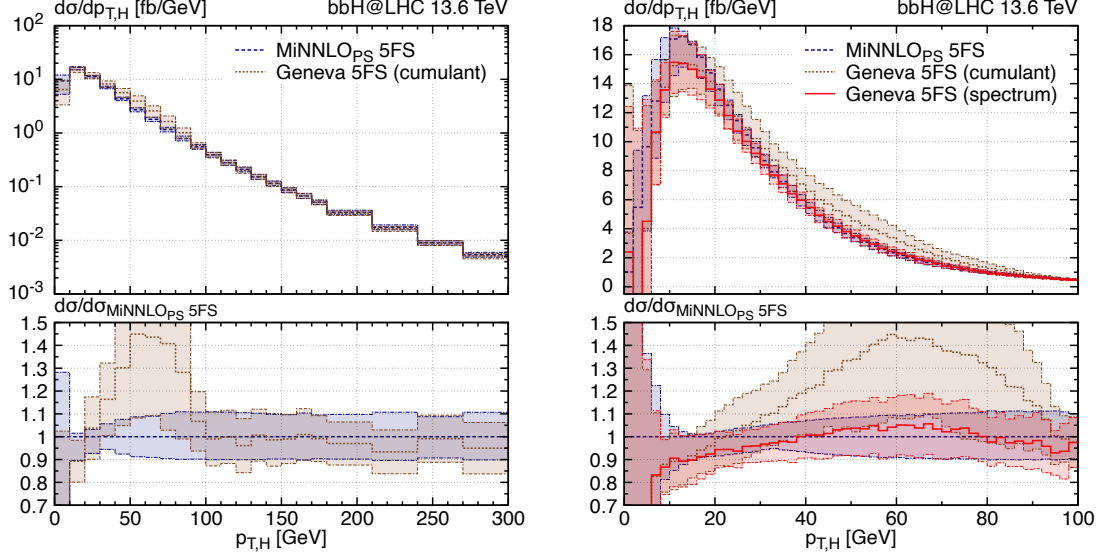
Figure 4: Comparison of MiNNLO$_{\text{PS}}$ (blue, dashed) and Geneva (brown, dotted) predictions at NNLO+PS level in the 5FS for the transverse momentum distribution of the Higgs boson, where Geneva uses their default cumulant scale choice. The zoomed version on the right shows also the alternative spectrum scale choice of the Geneva generator (red, solid).

We start the comparison by focusing on the transverse momentum spectrum of the Higgs boson in figure 4. The left plot shows the spectrum in a large range. As expected, we observe good agreement between MiNNLO$_{\text{PS}}$ and Geneva predictions at large transverse momenta, where both calculations are effectively NLO accurate and governed by H+jet production. Also in the range of $10-30$ GeV both generators yield relatively close results, consistent within their respective uncertainty. However, directly before and after the peak, and especially in the $30-100$ GeV range, we observe substantial differences between MiNNLO$_{\text{PS}}$ and Geneva with cumulant scale choice, barely covered by scale uncertainties, which are particularly large for Geneva in that range. The large difference in the transition region between Geneva with cumulant scale choices and MiNNLO$_{\text{PS}}$ is due to differences in the matching procedures. The analytic resummed prediction, used in the Geneva framework, underestimates the total cross section. However, this underestimated component must be included to obtain the correct total cross section. Since Geneva requires it to not affect either the peak region nor the fixed-order accuracy in the tail, it is accommodated in the matching procedure by modifying the transition region. In the Geneva matching procedure with the cumulant option, this leads to the observed larger scale uncertainties in the intermediate range of the $p_{\text{T},H} \sim [30, 90]$ GeV.

The right plot of figure 4 provides a zoomed-in view of the same observable and includes also the Geneva prediction obtained using the spectrum scale choices, as described in section 5.1.1, which are more appropriate for the transverse momentum spectrum. Moreover, in Geneva, the scale variation is implemented through variations of the profile scales at the spectrum level, making them particularly well-suited for transverse observables when using the spectrum scale
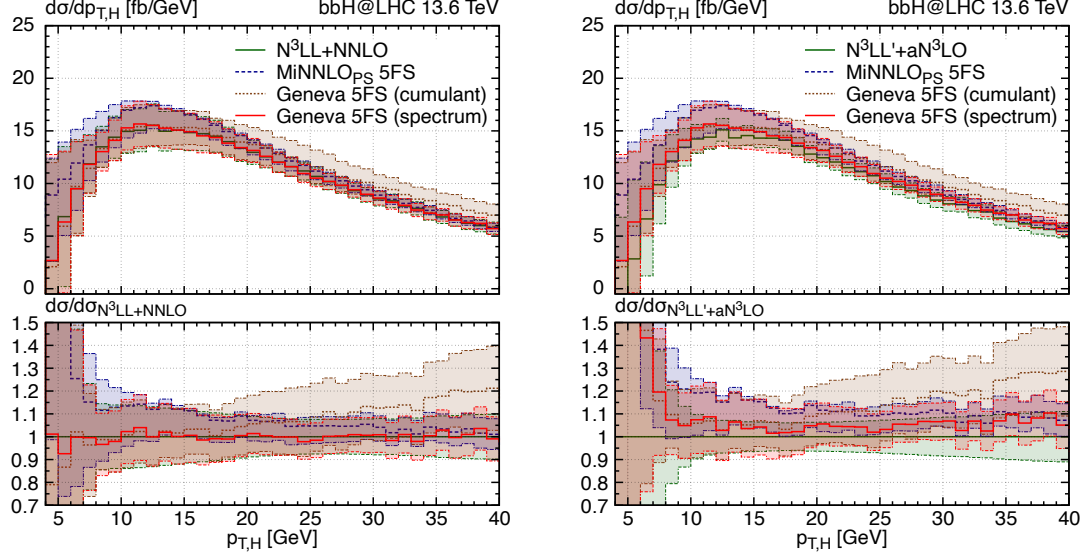
Figure 5: Comparison of the Higgs transverse momentum spectrum predicted by analytic resummed predictions (green, solid) at $N^3LL+NNLO$ (left plot) and at $N^3LL'+aN^3LO$ against the results obtained by the two MC generators: MiNNLO$_{PS}$ (blue, dashed) and GENEVA with cumulant (brown, dotted) and spectrum (red, solid) scale choices. All predictions are obtained in the 5FS for the y_b^2 contribution.

choice. Indeed, the substantial scale uncertainties observed for the cumulant scale choice in the matching region are strongly reduced for the spectrum scale choice, which features uncertainties that are of similar size as the MiNNLO$_{PS}$ ones. Most notably, we find that MiNNLO$_{PS}$ and GENEVA predictions are in significantly better agreement, when the spectrum scale choice is applied in GENEVA. In fact, the two predictions are in excellent agreement within their respective scale uncertainties over the entire transverse momentum range. We stress that at small transverse momenta all 5FS predictions become essentially unphysical, as power corrections in the bottom-quark mass become crucial for $p_T \lesssim m_b$, which are included only in 4FS calculations. Indeed, we observe that the scale uncertainty bands are severely inflated at small transverse momenta, and the predictions can even turn negative in the first bins, because the bottom PDFs are not valid below the bottom-quark mass threshold.

We compare the transverse momentum spectrum of the Higgs boson with the resummed analytic predictions discussed in section 4. In the left plot of figure 5, we show the MC predictions against the $N^3LL + NNLO$ result. By construction, the GENEVA prediction with the spectrum scale choice matches the analytic result exactly before the parton shower, and the shower does not introduce sizable numerical effects due to the local dipole recoil prescription selected in the shower settings of the calculations. On the other hand, the cumulant scale choice shows good agreement in the resummation region ($p_{T,H} < 20$ GeV), but begins to substantially deviate with increasing uncertainties at higher transverse momenta, as already observed in figure 4. The MiNNLO$_{PS}$ prediction also shows good agreement with $N^3LL + NNLO$ result within its scale
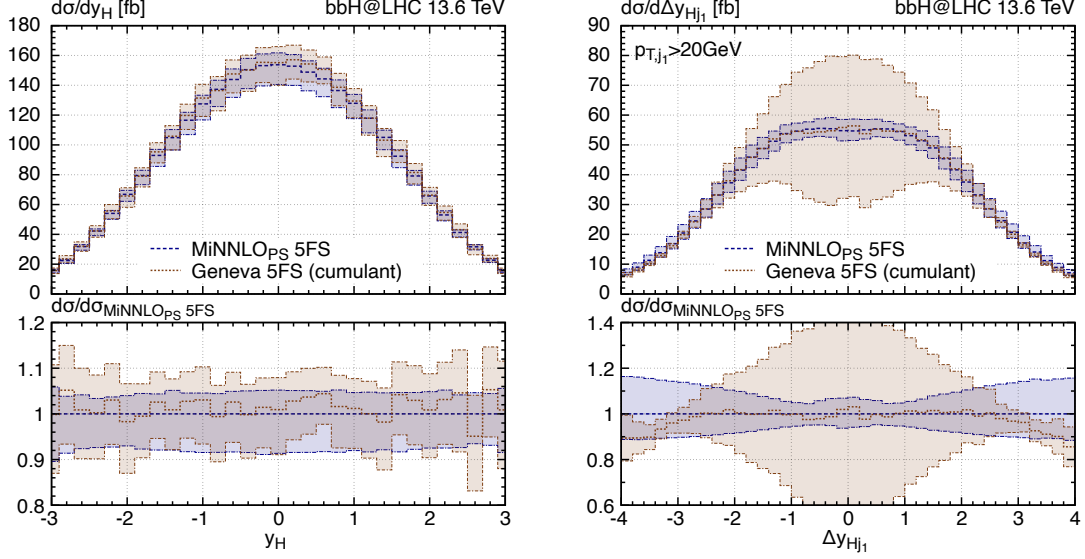
Figure 6: Higgs boson rapidity and difference in rapidity between the scalar and the leading jet as predicted by two MC generators in 5FS interfaced with Pythia8 using the MiNNLO$_{PS}$ (blue, dashed) and Geneva (brown, dotted) methods.

uncertainty band, with the largest deviations appearing at very low transverse momenta, well covered by the resummation scale variation. In that region, $p_T \lesssim m_b$, the massless calculation actually breaks down, and finite bottom-quark mass effects become relevant, as pointed out before. It therefore includes spurious effects induced by the PDF evolution, which turn the N^{3}LL$'$+NNLO cross section negative below $4\,$GeV, where the figure has been cut for that reason. In the right plot of figure 5, we present the comparison of the same MCs spectra against the N^{3}LL$'$+aN^{3}LO calculation. The inclusion of higher-order corrections in the analytic spectrum results in a negative shift relative to both the MiNNLO$_{PS}$ and Geneva predictions across the entire distribution, with a mostly flat effect for $p_{T,H} > 10,$GeV. Compared to the others, the Geneva prediction with the spectrum scale choice lies closer to the analytic result.

We conclude the section by presenting a comparison of two angular observables in figure 6. The left plot shows the NNLO-accurate Higgs rapidity distribution, displaying excellent agreement between the MiNNLO$_{PS}$ prediction and the Geneva result using the cumulant scale choice, in terms of shape, normalization and size of the scale uncertainties. The right plot illustrates an example of an observable that depends on the leading jet. Here, we apply a flavour-blind anti-k_T clustering algorithm with radius $R = 0.4$ and compute the rapidity difference between the Higgs boson and the highest-p_T jet, requiring a minimum jet transverse momentum of $20\,$GeV. We observe excellent agreement between the central MiNNLO$_{PS}$ and Geneva predictions, with some moderate differences only in the very forward region. However, the associated scale uncertainties differ significantly between the two generators, with Geneva exhibiting a much larger theoretical uncertainty at central rapidities.

5.1.3 Heavy-Higgs for BSM studies in MiNNLO$_{\text{PS}}$

Higgs boson production in association with a bottom-quark pair is of particular interest in BSM extensions. Indeed, many BSM scenarios predict modifications to the Higgs-bottom quark coupling, which could lead to observable deviations in the production rates and kinematic distributions of the $b\bar{b}H$ process. In many models, $b\bar{b}H$ production can become the dominant production mode of exotic Higgs states. The MiNNLO$_{\text{PS}}$ generator, introduced earlier in this section, is built within the SM framework, but can be easily extended to accommodate BSM predictions. To illustrate its potential, we consider a specific example of how the NNLO+PS generator can be adapted for BSM scenarios. We specifically consider the MSSM [107–112], which corresponds to a Type-II 2HDM [113] at LO, but deviates from it at higher orders. The MSSM enforces relations between the Higgs sector and the superpartners of SM particles. Unlike the SM, the MSSM requires two Higgs doublets (H_u and H_d) to give mass to both up-type and down-type fermions. An important parameter of the model is the ratio of vacuum expectation values (v_u and v_d) of the two SU(2) doublets,

$$\tan\beta = \frac{v_u}{v_d} \,. \tag{5.7}$$

The other independent parameter is the CP-even Higgs mixing angle α. This results in five physical Higgs bosons: two CP-even (h, H), one CP-odd (A) and two charged Higgs bosons ($H^{\pm}$). The lightest Higgs boson (h) in MSSM can mimic the SM Higgs, but has different properties depending on the model parameters. The tree-level mass of h is bounded from above by $m_Z|\cos 2\beta|$, where m_Z is the Z-boson mass. However, radiative corrections (mainly from the supersymmetric partners of the bottom and top quarks) can significantly alter the tree-level prediction, allowing for $m_h \sim 125\,\text{GeV}$ (see e.g. [114]). We perform the NNLO+PS prediction in the benchmark configuration known as M_h^{125} scenario [115], where all superparticles are chosen to be so heavy that the presence of these effects has only a mild impact on the production and decay of the light MSSM Higgs boson. Thus, the phenomenology of this scenario at the LHC closely resembles that of a Type-II 2HDM with Higgs couplings corresponding to the MSSM ones for light scalar states. On the other hand, for heavy bosons, there are large enhancements in the MSSM scenario. Loop corrections from Standard Model particles—dominated by the top-quark contribution—as well as from MSSM superpartners modify the effective bottom Yukawa coupling. The $\tan\beta$-enhanced SUSY corrections are resummed to all orders in the effective coupling. For the chosen mass of the SUSY partners, we refer to eq. (4) of ref. [115]. We stress that the NNLO+PS calculation in the 5FS scheme contains only terms proportional to the squared bottom Yukawa coupling. As a result, $b\bar{b}H$ predictions in the MSSM scenario differ from those in the SM—obtained with an heavy Higgs mass m_A—solely by an overall rescaling factor. Using chirality arguments, predictions for pseudo-scalar $b\bar{b}A$ production can be obtained from the $b\bar{b}h$ simulation by employing a heavy-boson mass and an effective Yukawa coupling, while neglecting the suppressed non-factorising SUSY-QCD corrections[5]. Therefore, in the case of the CP-odd Higgs boson production, we have:

$$\mathrm{d}\sigma_{b\bar{b}A}^{\text{MSSM}}(m_A) = \mathrm{d}\sigma_{b\bar{b}h}^{\text{SM}}(m_A) \cdot (\tilde{g}_b^A)^2 \,, \tag{5.8}$$

---

[5]The latter have been shown to be numerically small in ref. [116].
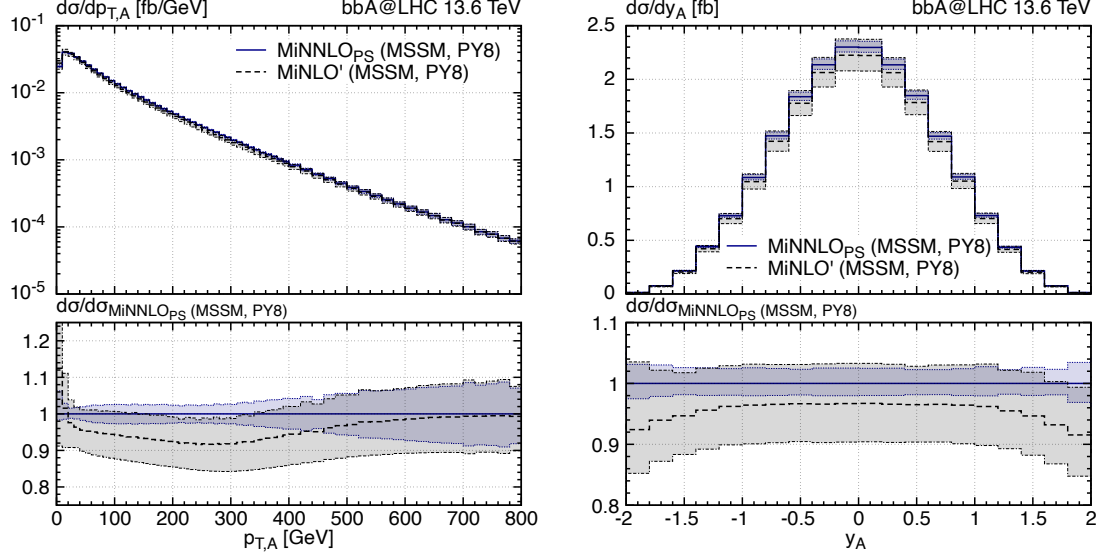
Figure 7: Comparison of MiNLO′ and MiNNLO_PS results for transverse momentum and rapidity distributions of the pseudo-scalar Higgs boson with $m_A = 1.4$ TeV and $\tan\beta = 20$.

with

$$\tilde{g}_b^A = \frac{\tan\beta}{1 + \Delta_b} \left(1 - \Delta_b \frac{1}{\tan^2\beta} \right) . \tag{5.9}$$

The parameter Δ_b resums higher-order sbottom contributions [117–121]. In ref. [121] the resummation effects has been studied in a systematic power-counting framework, estimating the uncertainties when keeping only the one-loop effects in the Δ_b determination. In order to reduce them, several two-loop calculations have been performed [122–125] and EW and diagonal contributions [126] have been computed recently. All these corrections have been incorporated into the resummation parameter Δ_b for this benchmark, with its numerical value determined using the `Hdecay` code [127, 128]. Following the current constraints on the M_h^{125} scenario, where the lightest Higgs has a mass of $m_h = 125$ GeV and is consistent with experimental observations, we consider the case of a CP-odd Higgs boson with a mass of 1.4 TeV and $\tan\beta = 20$, a point in the parameter space which is currently not excluded, as shown in Figure 1 of ref. [115]. We have performed the predictions by running the MiNNLO_PS 5FS generator with a heavy Higgs-boson mass and adjusted the Yukawa coupling according to eq. (5.8).

In figure 7, we present a comparison between MiNNLO_PS and MiNLO′ predictions. The left plot shows the transverse momentum spectrum. Due to the high mass of the bosonic state, the resummation region extends over a broader range of the transverse momentum spectrum compared to the SM Higgs, with a mass of 125 GeV. As a result, the NNLO corrections present in MiNNLO_PS have a larger impact even at intermediate transverse momentum values up to ~ 600 GeV, leading to more accurate predictions and smaller scale uncertainties for MiNNLO_PS compared to the MiNLO′ in a broad transverse momentum range. In the right plot of figure 7,
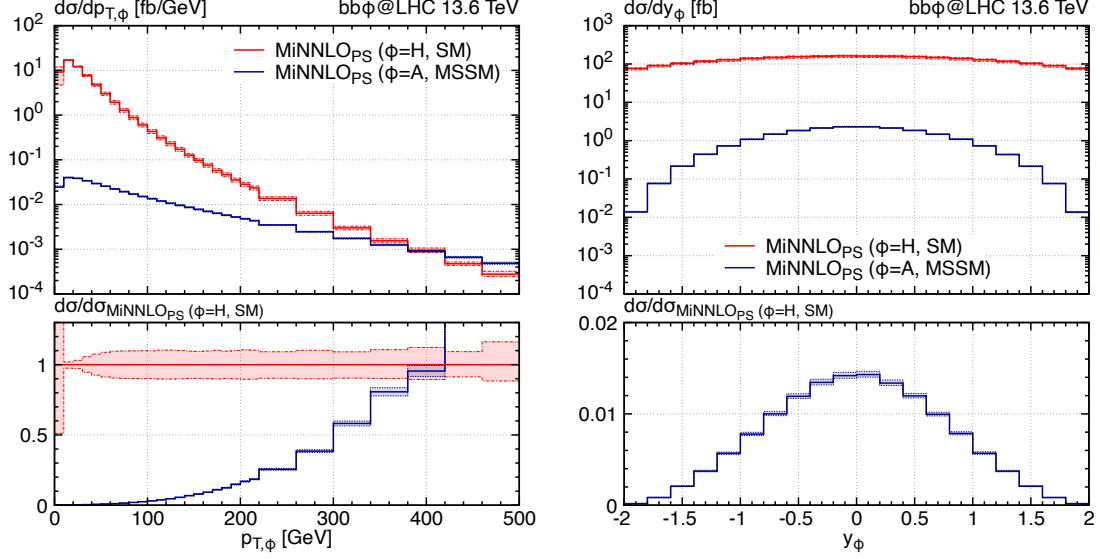
Figure 8: Higgs transverse momentum and rapidity spectra for MiNNLO_PS results with the heavy pseudo-scalar Higgs A compared to SM predictions.

we compare the two predictions for the Higgs rapidity spectrum: NNLO corrections increase the cross section with a flat correction in the central region $|y_A| < 1$. Notably, the NNLO effects encoded in MiNNLO_PS are positive in the case of a 1.4 TeV Higgs boson, compared to the SM case where the authors of ref. [17] have observed a flat negative correction in the Higgs rapidity spectrum.

Finally, we compare the differential behaviour of MiNNLO_PS predictions for the heavy Higgs state with the SM distributions in figure 8. In the left plot, we show the transverse momentum distribution. As expected, the BSM transverse momentum spectrum is substantially harder. With the chosen settings, BSM effects become even larger than the SM prediction for transverse momentum values greater than 400 GeV. In the right plot of figure 8, we compare the rapidity distributions. The heavy pseudo-scalar Higgs receives a larger contribution from central rapidities compared to the SM one, with the total contribution remaining always below 2% of the SM prediction. We stress that the numerical comparison is highly sensitive to the choice of the MSSM parameters. However, the purpose of this analysis is not to focus on a specific choice of the MSSM parameters, but to demonstrate the potential of the MiNNLO_PS generator for the modelling of a BSM signal of $b\bar{b}H$ production at NNLO+PS.

5.2 NNLO+PS predictions in 4FS

We now turn to NNLO+PS predictions computed in the massive 4FS for the y_b^2 component of $b\bar{b}H$ production, i.e. the corresponding 4FS calculation to the 5FS one presented in the previous section. Section 5.1 demonstrated that, in 5FS, the MiNNLO_PS and GENEVA procedures provide fully exclusive NNLO+PS results for the $b\bar{b}H$ process with massless bottom quarks. While that approach naturally resums collinear logarithms through the b-PDFs, it cannot account for power

corrections in m_b, which become particularly important at small Higgs transverse momenta. Moreover, the 4FS is better suited to model observables that depend on the b-jet kinematics.

5.2.1 MiNNLO$_{\text{PS}}$ method for $Q\bar{Q}F$ production

We consider a fully exclusive NNLO+PS generator for the $b\bar{b}H$ process in the 4FS [4]. This generator has been constructed using the extension of the MiNNLO$_{\text{PS}}$ method to heavy-quark–associated colour-singlet ($Q\bar{Q}F$) production, developed in ref. [103], which itself builds on the MiNNLO$_{\text{PS}}$ approach for $Q\bar{Q}$ production in ref. [100, 101]. While large logarithmic contributions at small transverse momentum in the $Q\bar{Q}F$ final state have the same general structure as for $Q\bar{Q}$ production, the more general kinematics of the $Q\bar{Q}F$ system, compared to the back-to-back configuration for $Q\bar{Q}$ production, has to be accounted for in the calculation of the coefficient functions for the resummation. The singular structure is governed by the factorization theorem, which is expressed in Fourier-conjugate (impact-parameter or b) space [129–132]:

$$\frac{\mathrm{d}\sigma}{\mathrm{d}^2\vec{p_{\mathrm{T}}}\,\mathrm{d}\Phi_{Q\bar{Q}\mathrm{F}}} = \sum_{c=q,\bar{q},g} \frac{|M_{c\bar{c}}^{(0)}|^2}{2m_{Q\bar{Q}\mathrm{F}}^2} \int \frac{\mathrm{d}^2\vec{b}}{(2\pi)^2} e^{i\vec{b}\cdot\vec{p_{\mathrm{T}}}} e^{-S_{c\bar{c}}\left(\frac{b_0}{b}\right)} \sum_{i,j} \mathrm{Tr}(\mathbf{H}_{c\bar{c}}\mathbf{\Delta})\,(C_{ci}\otimes f_i)\,(C_{\bar{c}j}\otimes f_j)\,, \tag{5.10}$$

where $|M_{c\bar{c}}^{(0)}|^2$ is the squared LO matrix element, $m_{Q\bar{Q}\mathrm{F}}$ the invariant mass of the $Q\bar{Q}\mathrm{F}$ system and $b_0 = 2e^{-\gamma_{\mathrm{E}}}$. The factor $e^{-S_{c\bar{c}}}$ represents the same Sudakov radiator that appears in the small-p_T resummation for colour-singlet production. In eq. (5.10), the sum over $c = q, \bar{q}, g$ spans all possible flavour assignments for the incoming partons, with the first parton carrying flavour c and the second parton carrying flavour $\bar{c}$. The collinear coefficient functions $C_{ij} = C_{ij}\big(z,\, p_1,\, p_2,\, \vec{b};\, \alpha_s(b_0/b)\big)$ arise from collinear emissions, which include also the constant terms, and the parton densities f_i are evaluated at the soft scale b_0/b. The composite factor $\mathrm{Tr}\big(\mathbf{H}_{c\bar{c}}\,\mathbf{\Delta}\big)\,\big(C_{ci}\otimes f_i\big)\,\big(C_{\bar{c}j}\otimes f_j\big)$ encodes the differences with respect to colour singlet production originating from the more involved colour structure and initial-final/final-final interferences for $Q\bar{Q}$ processes. It differs in its explicit form for the $q\bar{q}$ and gg channels and written symbolically here. In particular, this factor contains a nontrivial Lorentz structure—omitted here for brevity—that generates azimuthal correlations in the collinear limit [131, 133].

All quantities in bold face denote operators in colour space, and the trace $\mathrm{Tr}\big(\mathbf{H}_{c\bar{c}}\,\mathbf{\Delta}\big)$ in eq. (5.10) runs over colour indices. The hard function $\mathbf{H}_{c\bar{c}}$ is extracted from the infrared-subtracted amplitudes for $Q\bar{Q}F$ production, where the ambiguity in its definition corresponds to a choice of resummation scheme [134]. The operator $\mathbf{\Delta}$ encodes quantum interferences arising from soft radiation exchanged at large angles between the initial and final states, as well as among final-state quarks. It is given by $\mathbf{\Delta} = \mathbf{V}^\dagger \mathbf{D}\mathbf{V}$, where

$$\mathbf{V} = \mathcal{P}\exp\left\{-\int_{b_0^2/b^2}^{m_{Q\bar{Q}F}^2} \frac{dq^2}{q^2}\mathbf{\Gamma}_t(\Phi_{Q\bar{Q}F};\alpha_s(q))\right\}\,. \tag{5.11}$$

The symbol $\mathcal{P}$ denotes path ordering of the exponential matrix with respect to the integration variable q^2, arranging scales from left to right in increasing order. The anomalous dimension $\mathbf{\Gamma}_t$ governs the effect of real soft radiation emitted at large angles. Meanwhile, the azimuthal

operator $\mathbf{D} \equiv \mathbf{D}(\Phi_{Q\bar{Q}F}, \vec{b}, \alpha_s)$ encodes azimuthal correlations of the $Q\bar{Q}F$ system in the small-p_T limit. Upon averaging over the azimuthal angle ϕ, it satisfies $\left[\mathbf{D}\right]_\phi = \mathbf{1}$. Starting from the $Q\bar{Q}F$ resummation formula, the procedure to construct a MiNNLO$_{\text{PS}}$ improved $\bar{B}$ function system is the same as that of the colour-singlet case. All technical details of this derivation are provided in refs. [4, 100, 101, 103].

In the case of $b\bar{b}H$ production in the 4FS, the two-loop virtual corrections, required for NNLO accuracy, are not known in exact form with finite m_b. Instead, the two-loop amplitude is approximated in the NNLO+PS prediction by a small-mass expansion m_b, i.e. all logarithmically enhanced terms and constant terms are retained, while dropping terms that are power-suppressed in m_b. This massification procedure, developed in refs. [135, 136], allows us to capture the dominant virtual corrections in the small-m_b limit. The massless full-colour two-loop amplitudes, which provide the constant terms, are taken from ref. [137]. Different from the studies in ref. [4], which relied on the leading-colour approximation [138], here we perform a phenomenological analysis using events generated with the full-colour library of ref. [137] for the two-loop constant terms in the massification. The NNLO calculation is thus complete in full colour, up to power-suppressed terms in the bottom-quark mass, which are neglected only in the two-loop amplitude.

5.2.2 Results and flavour-scheme comparison

The setup for the phenomenological results presented here—including input parameters and PDFs—has been outlined in section 2. In addition, we specify the renormalization and factorization scale choices adopted in the MiNNLO$_{\text{PS}}$ simulations for the Born couplings. The Yukawa coupling is evaluated in the $\overline{\text{MS}}$ scheme at a scale of the Higgs mass

$$\mu_R^{(0),y_b} = m_H, \tag{5.12}$$

while the Born strong couplings are computed at a dynamical scale scale:

$$\mu_R^{(0),\alpha_s} = H_T/4, \quad \text{with} \quad H_T = M_{T,b} + M_{T,\bar{b}} + M_{T,H}, \tag{5.13}$$

where $M_{T,X} = \sqrt{M_X^2 + p_{T,X}^2}$ is the transverse mass of particle X.

We discuss the new theoretical predictions obtained at NNLO+PS in the 4FS for Higgs radiation off bottom quarks, and we compare them to the NNLO+PS results in the 5FS. We start by considering predictions of integrated cross sections in table 4. Apart from the fully inclusive cross section, we consider rates with identified b-jets, including a b-jet veto, the inclusive one- and two-b-jet rates. We define b-jets following the standard experimental definition, namely as anti-k_T jets that contain at least one bottom quark/B hadron. We apply a jet radius of $R = 0.4$, a minimum transverse momentum of $30\,\text{GeV}$ and a maximum absolute pseudo-rapidity of 2.4. Note that we have also considered a flavour-aware definition of b-jets using the *Interleaved Flavour Neutralization* (IFN) algorithm (with $\alpha = 2$ and $\omega = 1$) [139], which enables an infrared- and collinear-safe definition of anti-k_T b-jets also for fixed-order predictions in the massless scheme. Interestingly, we found that all numerical IFN results for the $b\bar{b}H$ process presented here differ by less than a few percent from the standard experimental definition, which is why we refrain from showing the IFN results and focus on the standard b-jet definition that is straightforward to apply in experimental analyses.

Looking at the total inclusive cross section in table 4, NNLO corrections in the 4FS increase the rate by about 30% relative to NLO. This highlights the importance of NNLO accuracy for precise predictions in the massive scheme. The MiNNLO$_{\rm PS}$ result in the 4FS shows a reduced dependence on the scale choices as compared to the NLO+PS prediction in the 4FS. Also the 5FS predictions, which correspond to the $b\bar{b} \to H + X$ process, receive sizable, but negative NNLO corrections of about -20%. Scale uncertainties are smaller in the 5FS, but they are significantly underestimated considering the fact that NLO and NNLO predictions do not agree within their respective uncertainties. At NLO, there is a severe discrepancy between the 4FS and 5FS cross sections, with the 5FS one being about 80% larger. By contrast, the NNLO+PS predictions in the two schemes agree well with each other within their respective scale uncertainties, due to the negative NNLO correction in the 5FS and the sizable positive correction in the 4FS. As a result, the long-standing tension between the 4FS and 5FS inclusive cross section is resolved once NNLO accuracy is included.

Considering the fiducial cross sections in the presence of b-jets in table 4, we observe that about 80% of the events are produced in the 0-b-jet bin. This result is consistent between the 4FS and 5FS NNLO+PS predictions. By contrast, at NLO+PS the 5FS predictions a fraction of 85% of events with no b-jets. Requiring at least one b-jet leads to a significant reduction in the cross section by a factor of approximately 5, i.e. about 20% of the events have one or more b-jets. Requiring a second b-jet further suppresses the rate by roughly an additional order of magnitude, with about 1.4% of the $b\bar{b}H$ events having two or more b-jets. These relative b-jet acceptances are in remarkable agreement between the 4FS and 5FS NNLO+PS generators (in fact, also compared to the 4FS NLO+PS generator), while the 5FS NLO+PS predictions being quite different. It is reassuring to observe this high level of agreement, despite the fact that in the 5FS the accuracy effectively reduces by one order for each required b-jet, whereas the 4FS predictions remain genuinely NNLO accurate in all considered b-jet categories. Note that for the MiNNLO$_{\rm PS}$ 4FS predictions the inclusive cross section and 0-b-jet bin feature larger uncertainties that the more exclusive 2-b-jet selection, which could be related to a lower sensitivity to logarithmic corrections in the bottom-quark mass when two hard b-jets are required. Also for the absolute cross section numbers at NNLO+PS in the 4FS and 5FS, the inclusion of higher-order corrections via MiNNLO$_{\rm PS}$ improves the overall consistency between the two

Fiducial region	NLO$_{\rm PS}$ 5FS	NLO$_{\rm PS}$ 4FS	MiNNLO$_{\rm PS}$ 5FS	MiNNLO$_{\rm PS}$ 4FS
inclusive	$725.4(2)^{+11\%}_{-10\%}$ fb	$389.0(1)^{+24\%}_{-20\%}$ fb	$574.8(4)^{+4.5\%}_{-8.0\%}$ fb	$519.6(3)^{+19\%}_{-15\%}$ fb
H $+$ 0 b-jets	$619.5(9)^{+11\%}_{-10\%}$ fb	$312.1(4)^{+23\%}_{-20\%}$ fb	$458.1(3)^{+3.3\%}_{-7.8\%}$ fb	$420.2(2)^{+21\%}_{-15\%}$ fb
H $+ \geq 1\,b$-jets	$105.9(1)^{+10\%}_{-10\%}$ fb	$76.91(6)^{+26\%}_{-20\%}$ fb	$116.7(1)^{+9.4\%}_{-8.7\%}$ fb	$99.38(2)^{+7.5\%}_{-12\%}$ fb
H $+ \geq 2\,b$-jets	$5.992(3)^{+10\%}_{-10\%}$ fb	$5.116(2)^{+32\%}_{-23\%}$ fb	$8.621(3)^{+11\%}_{-10\%}$ fb	$7.154(6)^{+1.7\%}_{-10\%}$ fb

Table 4: Predictions for cross section rates in fb of different Powheg and MiNNLO$_{\rm PS}$ generators in the 4FS and 5FS for the y_b^2 contribution.
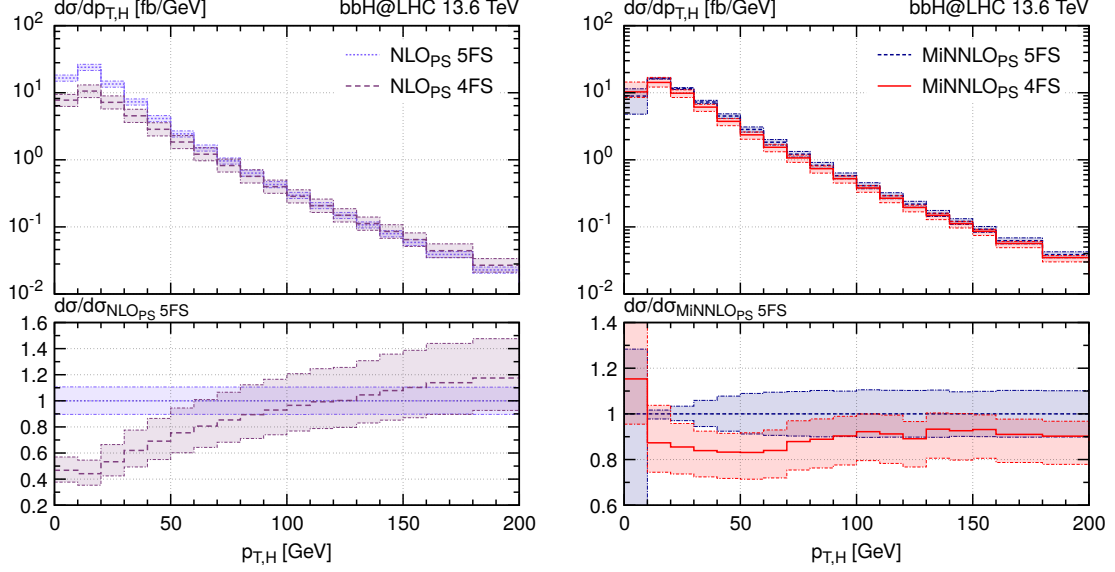
Figure 9: Comparison between different flavour scheme choices for the Higgs transverse momentum spectrum at NLO+PS (left) and NNLO+PS level (right) for the y_b^2 contribution.

schemes considerably, especially in the b-jet-vetoed cross sections, which are a factor of two apart in the NLO-accurate predictions. Similarly, the one(two)-b-jet cross section at NNLO+PS, which is only NLO-accurate (LO-accurate) in the 5FS, is in good agreement with the 4FS one, as soon as the MiNNLO$_{PS}$ corrections are included.

Next, we compare differential distributions in 4FS and 5FS at NLO+PS and NNLO+PS in figure 9 and 10. We show the Higgs transverse momentum distribution in figure 9. The left plot shows the NLO+PS predictions and the right plot the NNLO+PS ones. At NLO+PS, the 4FS and 5FS predictions differ significantly at low $p_{T,H}$, featuring an entirely different shape. At NNLO+PS, this discrepancy is significantly reduced: MiNNLO$_{PS}$ matching brings the two predictions into much better agreement across the full $p_{T,H}$ range. Disregarding the 10% difference in the normalization that was already observed for the total inclusive cross section, the shape of the two distributions is very similar, with the exception of the first bin, where the 5FS provides an invalid description, as discussed before. To be more precise, for $p_{T,H} \gtrsim 70\,\text{GeV}$ the ratio of the two predictions is very flat, while for $p_{T,H} \lesssim 70\,\text{GeV}$ we observe shape variations of about 5%. In all cases, 4FS and 5FS predictions are consistent within uncertainties.

Figure 10 shows the Higgs transverse momentum distribution in events with at least one (left) or two (right) b-jets identified. For the inclusive one-b-jet selection, the differences between the schemes are moderate and largely flat, except in the small $p_{T,H}$ region, where they reach up to 20%, slightly beyond the respective uncertainties. In the two-b-jet category, the differences at small $p_{T,H}$ increase, with the 4FS prediction being systematically lower than the 5FS one. This behaviour reflects the more accurate treatment of bottom-quark kinematics in the massive scheme, which becomes particularly relevant when two b-jets are required to be hard and well separated. These configurations are effectively described only at LO+PS accuracy in the 5FS.
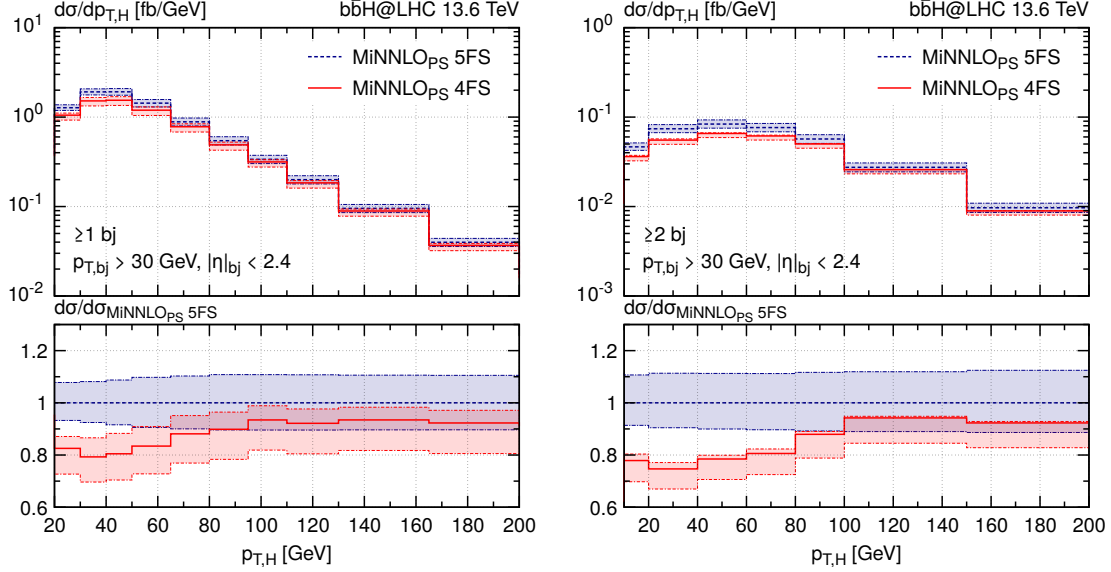
Figure 10: Higgs transverse momentum spectrum with at least one (left plot) or two (right plot) b-jets identified using the experimental-like algorithm applied to the events generated by MiNNLO$_{\rm PS}$ in the massless (blue, dashed) and massive (red, solid) schemes for the y_b^2 contribution.

These results underline the importance of the 4FS computation for observables involving identified b-jets. Due to the partonic structure of the 5FS calculation, it lacks accuracy in the hard matrix-element description of b-jet multiplicities compared to the 4FS, which in all observables involving up to two b-jets retains the full NNLO+PS accuracy. As a result, the 4FS provides a more reliable and accurate prediction, especially in regions sensitive to the kinematics and multiplicity of b-jets. This makes the 4FS prediction highly relevant for comparisons with experimental measurements involving b-tagged final states.

6 Modelling of the $b\bar{b}H$ background in HH searches

6.1 Comparison of different $b\bar{b}H$ generators for y_t^2 and y_b^2 contributions

In this section, we study $b\bar{b}H$ production as a background to di-Higgs searches at the LHC. To this end, we consider MC predictions for both the y_t^2 and y_b^2 contributions to the $b\bar{b}H$ cross section with fiducial selections relevant to enhance a HH signal at the LHC [140, 141].[6] Our study closely follows the work presented in ref. [23], with the main differences being the updated collider energy and input parameters, as described in section 2, as well as novel predictions for the y_b^2 component computed at NNLO+PS in the 4FS using the MiNNLO$_{\rm PS}$ generator [4]. The y_t^2 predictions are provided in the 4FS at NLO QCD accuracy matched to the PYTHIA8 [142] parton shower. The

---

[6]The $y_t y_b$ interference contribution is about -10% at NLO+PS, which is less than the respective scale uncertainties of the y_b^2 and y_t^2 cross section. It therefore does not play a relevant role for the considerations in this section and can be safely neglected.

results are obtained automatically with MADGRAPH5_AMC@NLO [143, 144] using the NLO calculation of ref. [22] (in particular of the virtual amplitude in the HTL).

We compare the y_t^2 predictions to those from an inclusive gluon-fusion NNLOPS simulation [18–20] in the 5FS[7], generated using POWHEG_BOX_V2 [104, 105, 145]. This setup achieves NNLO accuracy for inclusive Higgs boson observables, but only provides LO accuracy for final states in which the Higgs boson is produced in association with two additional b-jets. In the NNLOPS calculation, the renormalization and factorization scales are set to $\mu_R = \mu_F = m_H/2$, the PDF4LHC21 parton distribution functions are used [28], and PYTHIA8 is employed both for parton showering and for simulating the decay of the Higgs boson into two photons, which are kept stable in the showering process.

The HH signal region is inspired by the $HH \to b\bar{b}\gamma\gamma$ final state [146, 147]. Specifically, we require two b-tagged anti-k_T [148–150] jets with a radius of $R = 0.4$ satisfying

$$p_T(j) > 25\,\text{GeV} \qquad \text{and} \qquad |\eta(j)| < 2.5\,, \tag{6.1}$$

with their invariant mass constrained to be compatible with the Higgs boson mass:

$$80\,\text{GeV} < m(b_1, b_2) < 140\,\text{GeV}\,. \tag{6.2}$$

Additionally, we require two photons—produced in the simulation via Higgs decays through PYTHIA8—to pass the following selection criteria:[8]

$$105\,\text{GeV} < m(\gamma_1, \gamma_2) < 160\,\text{GeV}, \quad |\eta(\gamma_i)| < 2.37, \quad \frac{p_T(\gamma_1)}{m(\gamma_1, \gamma_2)} > 0.35, \quad \frac{p_T(\gamma_2)}{m(\gamma_1, \gamma_2)} > 0.25\,. \tag{6.3}$$

The presence of two b-jets and two photons satisfying the above requirements defines the *fiducial* region. This selection can be further refined in the context of HH analyses by imposing a cut on the variable

$$m_{2b2\gamma}^{\star} = m_{2b2\gamma} - m(b_1, b_2) - m(\gamma_1, \gamma_2) + 2m_H\,. \tag{6.4}$$

This observable is used in HH searches [146, 147, 151, 152] to define selection cuts that enhance the sensitivity to an anomalous trilinear Higgs coupling. Here, we consider two scenarios in which the fiducial selection includes the requirements $m_{2b2\gamma}^{\star} < 500\,\text{GeV}$ and $m_{2b2\gamma}^{\star} < 350\,\text{GeV}$, respectively.

We present inclusive and fiducial cross section yields in table 5. We start by comparing the numerical results for $b\bar{b}H$ y_t^2 component, computed at NLO in the 4FS using MADGRAPH5_AMC@NLO (first column), with the expected rate obtained from the NNLOPS simulation, with (second column) and without $g \to b\bar{b}$ splitting included in the parton shower (third column). All rates include the Higgs branching ratio into photons, $\text{BR}(H \to \gamma\gamma) = 0.227\%$ [27].

---

[7]The so-called NNLOPS simulation [18–20] is based on an a posteriori reweighting of MiNLO′ events to reach NNLO-accuracy for Born-level observables, i.e. those related to the colour-singlet final state. By contrast, the previously discussed MiNNLO$_{\text{PS}}$ method incorporates the additional terms required to achieve NNLO accuracy directly in the event generation.

[8]Note that, since we employ the Higgs decay in the zero-width approximation, the Higgs boson is on-shell and the invariant mass of the two photons is exactly equal to Higgs mass $m(\gamma_1, \gamma_2) = m_H$, which trivially fulfils the first condition and simplifies the other ones.

Uncertainties due to renormalization and factorization scale variations are quoted, where each scale is independently varied by a factor of two around the central value following the 9-point prescription. The theoretical uncertainty in this section is estimated from the envelope of the nine scale variations, following ref. [23], in contrast to the other sections where the standard 7-point prescription with the constraint $1/2 \leq \mu_R/\mu_F \leq 2$ is employed. Considering 7-point variations has a very small effect on the scale-uncertainty band for the total rates, and we have decided to align the choices with the previous HH-background studies [23]. Additional theoretical uncertainties, such as those associated with variations of the shower starting scale, the choice of parton shower algorithm, or modifications to the MC@NLO matching procedure [153, 154] were examined in ref. [23] and found to be subleading. NNLOPS uncertainties are evaluated via multiple sources, accounting for the modelling of jet multiplicity, the Higgs boson $p_{T,H}$, $p_{T,Hjj}$, and m_{jj} [27, 155–159], as discussed in ref. [160]. Parton shower uncertanties are also not shown for the NNLOPS prediction, but they are expected to be sizeable: a comparison with an alternative parton shower (HERWIG7 [161]) yields differences in the fiducial $b\bar{b}H$ (y_t^2) cross section ranging from 3% up to 17% (depending on the kinematic region).

Significant differences are observed between the MADGRAPH5_AMC@NLO predictions and the NNLOPS ones, with the NNLOPS fiducial cross section up to twice as large (depending on the kinematical selections) when the $g \to b\bar{b}$ splittings are included in the parton shower. As discussed in ref. [23], the parton shower induces a double counting of $gg \to H + 2$ b-jets contributions, by dressing the inclusive production of the Higgs boson with hard b-jet radiation, which are also included at the hard matrix-element level in the NNLOPS calculation. Those hard configurations are formally outside the validity range of a parton shower, which is based on soft/collinear factorization. This mismodelling created by the NNLOPS sample is currently covered by a conservative 100% uncertainty in HH analyses [146, 152]. Given that $b\bar{b}H$ production is the major background, reducing this uncertainty through more accurate simulations for the y_t^2 contribution to the $b\bar{b}H$ background will be instrumental for future HH measurements.

We also quote the rates for the $b\bar{b}H$ y_b^2 component in table 5 (last column), which are evaluated at NNLO+PS accuracy with the MINNLO$_{PS}$ generator introduced in section 5.2.1. In all fiducial HH categories, the y_b^2 and y_t^2 contributions to the $b\bar{b}H$ cross section are of the same

Fiducial region	y_t^2 NLO (NLO+PS)	y_t^2 LO (ggF NNLOPS)	y_t^2 LO $g \to b\bar{b}$ (ggF NNLOPS)	y_b^2 NNLO ($b\bar{b}H$ MINNLO$_{PS}$)
No cut	$1696^{+62\%}_{-35\%}$ ab	$7574^{+8\%}_{-8\%}$ ab	$2774^{+7\%}_{-7\%}$ ab	$1180^{+19\%}_{-15\%}$ ab
Fid. cuts	$18^{+55\%}_{-33\%}$ ab	$31.6^{+18\%}_{-18\%}$ ab	$20.5^{+18\%}_{-18\%}$ ab	$5.6^{+2.8\%}_{-10\%}$ ab
Fid. cuts + $m^\star_{2b2\gamma} < 500\,\text{GeV}$	$12^{+57\%}_{-33\%}$ ab	$23.3^{+20\%}_{-20\%}$ ab	$15.4^{+20\%}_{-20\%}$ ab	$5.5^{+2.8\%}_{-10\%}$ ab
Fid. cuts + $m^\star_{2b2\gamma} < 350\,\text{GeV}$	$5.5^{+60\%}_{-34\%}$ ab	$11.5^{+20\%}_{-20\%}$ ab	$7.76^{+20\%}_{-20\%}$ ab	$4.8^{+3.1\%}_{-10\%}$ ab

Table 5: Cross sections in ab for the y_t^2 and y_b^2 contributions to $pp \to b\bar{b}H$ with $H \to \gamma\gamma$ decay at $\sqrt{s} = 13.6$ TeV.

order as the HH signal cross section [23] (not included in the table), highlighting the importance of their accurate modelling to obtain a precise measurement of the HH process. The y_t^2 term is larger than the y_b^2 contribution to the $b\bar{b}H$ cross section for the inclusive cross section (by about 50%) and in the fiducial region without $m_{2b2\gamma}^\star$ cut (by a factor of about three). With kinematical selections on $m_{2b2\gamma}^\star$, however, the relative contribution of the y_b^2 component increases. For the fiducial region with $m_{2b2\gamma}^\star < 500\,\mathrm{GeV}$, the y_t^2 term is larger by roughly a factor of two, while for $m_{2b2\gamma}^\star < 350\,\mathrm{GeV}$ y_b^2 and y_t^2 contributions are already comparably large. The latter is the fiducial region most sensitive to the trilinear Higgs coupling. Hence, the accurate modelling of both, y_b^2 and y_t^2 components, is important to fully control the $b\bar{b}H$ background.

We continue by considering differential distributions in the HH signal region in figure 11 and 12, including the Higgs transverse momentum spectrum (left figures) and the $m_{2b2\gamma}^\star$ distribution (right figures). For the y_b^2 component in figure 11 we compare 4FS predictions at NLO+PS and NNLO+PS. We find that the inclusion of NNLO corrections increases the cross section 40–60% and leads to a significant reduction in the scale uncertainties. Although the NNLO correction in $m_{2b2\gamma}^\star$ is rather flat, it is clear that for a precise description of the y_b^2 cross section of $b\bar{b}H$ production NNLO-accurate predictions in the 4FS are indispensable. In figure 12 [162] we compare the y_t^2 predictions from the MADGRAPH5_AMC@NLO and NNLOPS samples, after applying only the b-jet selection defined in eq. (6.1). The distributions are normalised to unity in order to highlight that the 4FS NLO+PS MADGRAPH5_AMC@NLO generator predicts a significantly harder spectrum than the 5FS LO+PS prediction from the NNLOPS generator. By normalising to unity, these shape effects are disentangled from the even larger rate differences with respect to NNLOPS, discussed before.

6.2 Combining y_t^2 $b\bar{b}H$ component and inclusive Higgs boson production in the 4FS

In analyses focusing on final states containing b-jets, it is essential to accurately model the contributions from light-flavour and charm jets that may enter the event selection due to mistagging. To facilitate the use of the MADGRAPH5_AMC@NLO sample in experimental studies, while maintaining a realistic description of all jet flavour components, the y_t^2 contribution to the $b\bar{b}H$ process at NLO+PS is supplemented with the inclusive Higgs boson production sample (including higher-order light-jet multiplicities) provided by the NNLOPS generator, consistently within the 4FS. The NNLOPS simulation includes the inclusive description of the $gg \to H$ process at NNLO, but also describes one accompanied light-flavour and charm jets at NLO and two of them at LO, which are not represented in the MADGRAPH5_AMC@NLO sample for $b\bar{b}H$ production.

To prevent double counting of events featuring $gg \to H$ production with two b-jets, the NNLOPS sample is filtered to exclude any event that contains *at least* one bottom quark, regardless whether it originates from the hard scattering or from parton showering. Removing events with a single bottom quark from the NNLOPS sample ensures complete orthogonality of configurations between the two samples. This excludes $gb \to bH$ contributions, which are already accounted for in the MADGRAPH5_AMC@NLO prediction via initial-state $g \to b\bar{b}$ splittings. Thus, by effectively removing the $b\bar{b}H$ component from the NNLOPS sample, it is turned into a 4FS description of Higgs boson production accompanied by only light jets. The filtered NNLOPS sample can then be combined with the MADGRAPH5_AMC@NLO one for
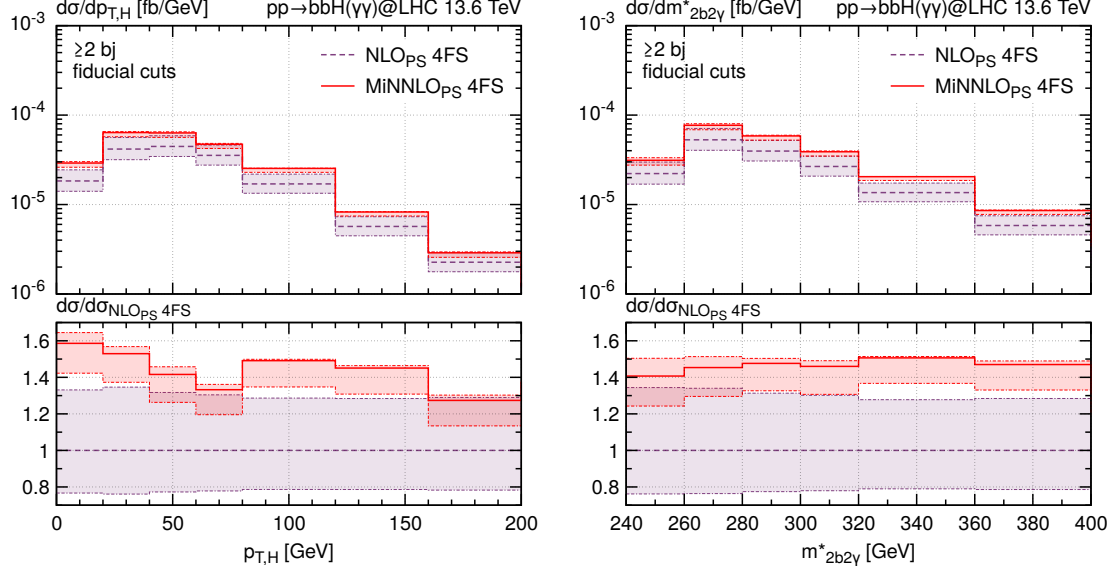
Figure 11: Transverse momentum spectrum of the Higgs boson and invariant mass $m_{2b2\gamma}^{\star}$ as defined in eq. (6.4) in the fiducial volume described by the selections (6.1-6.3), comparing NLO+PS (purple, dashed) and NNLO+PS (red, solid) 4FS predictions for the y_b^2 contribution.
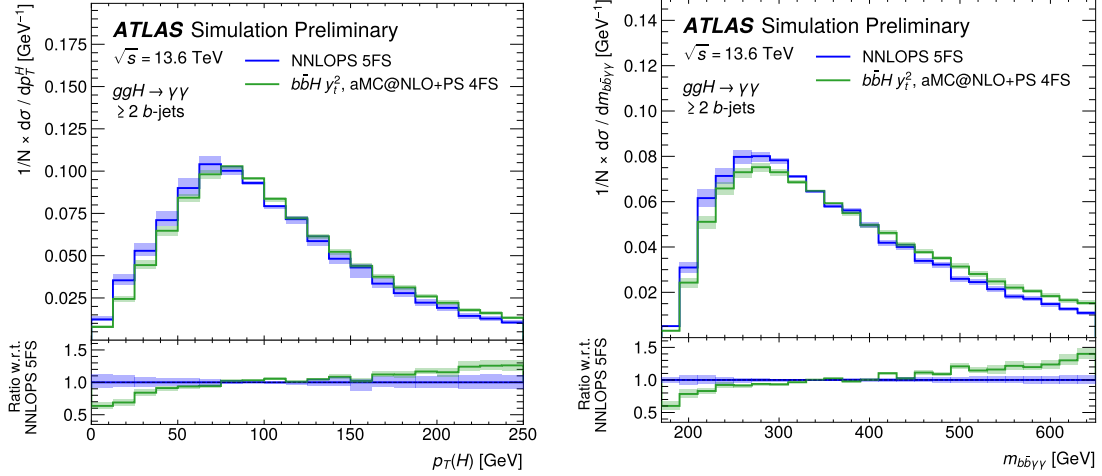
Figure 12: Distributions of the Higgs boson p_{T}, and invariant mass $m_{2b2\gamma}^{\star}$ as defined in eq. (6.4) for the y_t^2 contribution predicted by MADGRAPH5_AMC@NLO and NNLOPS samples after requiring at least 2 b-jets in the final state as described by eq. (6.1). All distributions are normalised to unity. The blue and green shaded bands represent the scale uncertainties (shape only) of the NNLOPS and MADGRAPH5_AMC@NLO samples, respectively. The lower panel displays the ratio of the two predictions. [162]

$b\bar{b}H$ production at NLO+PS by simply adding the two contributions, obtaining a full description of Higgs boson production with light- and b-jet final final states within the 4FS, where inclusive Higgs observables are described at NNLO+PS and H+b-jet final states at NLO+PS. Although this method combines a 4FS calculation with one that was originally obtained in the 5FS, by dropping consistently all bottom-quark contributions in the NNLOPS prediction, it is turned effectively into a 4FS calculation.

One should bear in mind, however, that for full consistency also the PDFs and strong coupling need to be updated to 4FS ones within this calculation. In order to exploit the existing NNLOPS samples, this is not done here for practical reasons. Still, even with this caveat, the method outlined above provides a coherent and practical approach for estimating the $gg \to H$+b-jets contribution at analysis level. This strategy has already been used in similar contexts, such as the modelling of Z boson production with two bottom quarks in ref. [163], and the treatment of the $t\bar{t} + b\bar{b}$ process in ref. [164]. As discussed in ref. [162], the filtering efficiency, defined as the fraction of NNLOPS events surviving the bottom quark veto, is found to be 94%. The filtered NNLOPS sample is then normalised to the inclusive $gg \to H$ cross section at N^{3}LO after subtracting the y_t^2 $b\bar{b}H$ component as listed in table 6. The comparison of nominal and filtered NNLOPS samples is discussed in ref. [162].

7 Light-quark Yukawa contributions to Higgs boson production

The cross section proportional to the bottom-quark Yukawa coupling yields the largest (and most relevant) quark-induced contribution to Higgs boson production after the top quark. However, Higgs boson production mechanisms induced by the lighter quarks (charm, strange, up, down) play an important role to constrain the light-quark Yukawa couplings. Indeed, while the bottom-quark Yukawa coupling is strongly constrained through measurements of Higgs decays, no stringent bounds exist for lighter quarks [165]. In particular, the charm Yukawa coupling is only weakly constrained, with an observed upper limit of less than 8.5 times the SM prediction based on analyses of Higgs decay products in Higgsstrahlung events [166]. Light-quark Yukawa contributions typically have an important impact at small momentum-transfers, for instance, at small transverse momentum of the Higgs boson. Therefore, ref. [38] suggested to access the

$\sqrt{s}$	σ	$\Delta_{(\mu_R, \mu_F)}$	Δ_{PDF}
13.0 TeV	667 fb	$+62\%/-35\%$	$\pm 1.7\%$
13.6 TeV	723 fb	$+62\%/-36\%$	$\pm 1.7\%$
14.0 TeV	763 fb	$+62\%/-36\%$	$\pm 1.7\%$

Table 6: Total $b\bar{b}H$ cross sections for the y_t^2 contribution in the SM at LHC center-of-mass energies of $\sqrt{s} = 13$ TeV, 13.6 TeV, and 14 TeV. The cross sections are evaluated for a Higgs mass of $m_h = 125$ GeV and the PDF4LHC21_40_nf4 (LHAPDF ID 93500) set is employed for the parton distribution functions. Variations in the cross section due to changes in m_h between 125 GeV and 125.20 GeV are negligible compared to the scale uncertainty.

bottom and charm Yukawa couplings through precise measurements of the Higgs transverse momentum distribution.

The Higgs boson production mechanisms induced by light-quark Yukawa couplings correspond precisely to the ones of $b\bar{b}H$ production, with one contribution coming from loop-induced gluon fusion, while another coming from the tree-level production of the Higgs boson in association with light quarks. Again different prescription of treating the quarks as massless or massive can be considered. However, for the lighter quark flavours, the treatment as massless objects is more suitable in general. As for $b\bar{b}H$ production, the typical tree-level production mode in the massless scheme is the quark-fusion process $q\bar{q} \to H$ with $q \in \{b, c, s, u, d\}$, and we write the cross section as follows:

$$\sigma_{q\bar{q}\to H}(\bar{\kappa}_q^2) = \sigma_{b\bar{b}\to H} + \bar{\kappa}_c^2 \bar{\sigma}_{c\bar{c}\to H} + \bar{\kappa}_s^2 \bar{\sigma}_{s\bar{s}\to H} + \bar{\kappa}_d^2 \bar{\sigma}_{d\bar{d}\to H} + \bar{\kappa}_u^2 \bar{\sigma}_{u\bar{u}\to H} \,. \tag{7.1}$$

All interference effects at higher orders are mass suppressed, and they vanish in the massless treatment with $n_f = 5$. We have introduced the coupling $\bar{\kappa}_q = y_q(m_H)/y_b(m_H)$, which denotes the ratio of the Yukawa coupling of a light quark to the SM Yukawa coupling of the bottom quark, both evaluated in the $\overline{\text{MS}}$ scheme at the scale m_H, and the cross section with the corresponding Yukawa coupling stripped off, $\bar{\sigma}_{q\bar{q}\to H} = \sigma_{q\bar{q}\to H} \cdot y_b^2(m_H)/y_q^2(m_H)$. In other words, the cross sections in eq. (7.1) are obtained using the appropriate quark PDF, while assigning the Yukawa interaction to the strength of the bottom-quark coupling. This is done here to obtain cross sections of comparable size.

A value of $\bar{\kappa}_q = 1$ corresponds to a Yukawa coupling for quark q equal in strength to that of the bottom quark. Thus, the normalised couplings take the following values in the SM: $\bar{\kappa}_b = 1$, $\bar{\kappa}_c \simeq 2.3 \cdot 10^{-1}$, $\bar{\kappa}_s \simeq 1.9 \cdot 10^{-2}$, $\bar{\kappa}_d \simeq 2.7 \cdot 10^{-3}$, $\bar{\kappa}_u \simeq 4.4 \cdot 10^{-4}$. The numerical values are obtained by using the PDG values of the quark masses in the $\overline{\text{MS}}$ scheme [31] as boundary conditions and evolving them to the hard scale m_H using four-loop running. The High-Luminosity LHC prospects [167] show that the light-quark Yukawa coupling can be constrained to $|\bar{\kappa}_c| \leq 3.34$, $|\bar{\kappa}_d| \leq 0.39$, $|\bar{\kappa}_u| \leq 0.33$ at 95% Confidence Level when using kinematical distributions, in particular the transverse momentum spectrum. In ref. [167] other methods for constraining light quark Yukawa couplings, such as exclusive decays, have been discussed, leading to an global expectation of $|\bar{\kappa}_c| \leq 0.52$, $|\bar{\kappa}_s| \leq 0.31$, $|\bar{\kappa}_d| \leq 0.34$, $|\bar{\kappa}_u| \leq 0.33$.

We present results for Higgs boson production induced by light-quark Yukawa interactions based on two different calculations: the NNLO+PS calculation for $b\bar{b} \to H$ production with MiNNLO$_{\text{PS}}$ in ref. [17], which has been extended to all light-quark fusion processes; and the resummed N^{3}LL$'$+aN^{3}LO predictions in ref. [40], which have been obtained not only for $b\bar{b} \to H$, but also for $c\bar{c} \to H$ and $s\bar{s} \to H$ production in that work. The latter calculation has also been used to construct the Geneva NNLO+PS generator for the $c\bar{c}H$ process in ref. [16], which will not be studied here.

In the following, we consider the Higgs transverse momentum spectrum, as one of the observables most sensitive to light-quark Yukawa interactions, especially at small transverse momentum, and present results at both NNLO+PS level from the MiNNLO$_{\text{PS}}$ generator and for the N^{3}LL$'$+aN^{3}LO resummed spectrum. We further apply the MiNNLO$_{\text{PS}}$ simulation to a detailed phenomenological study at NNLO+PS level in the diphoton channel $q\bar{q} \to H \to \gamma\gamma$, where we include the Higgs decay to two photons through the Pythia8 parton shower.

7.1 Sensitivity of the Higgs p_T spectrum to light-quark Yukawa couplings

We begin with the transverse momentum spectrum of the Higgs boson. In figure 13, we show the normalised distribution for the five different flavour channels obtained from the MiNNLO$_{\rm PS}$ generator (in the left plot) and for the second-/third-generation quark channels at N^{3}LL$'$+aN^{3}LO (in the right plot).[9] By normalising to the total cross section, we remove the dependence on the Yukawa coupling, making the comparison sensitive only to differences in the parton distributions in each channel. We observe that the position of the peak varies significantly with the initial-state flavour, with light-quark channels exhibiting the softest spectrum and the bottom quarks the hardest one. The comparatively hard spectrum in the bottom-quark channel is a consequence of the bottom-quark PDF being generated perturbatively and predominantly from gluon splittings.

Although the small masses of the first- and second-generation quarks make their contributions challenging to detect experimentally, the shape of the Higgs transverse momentum distribution provides a potential handle to disentangle them from the dominant gluon-fusion channel, which features a much harder spectrum, peaked at larger values, and therefore distributes the cross section towards large transverse momentum values. In particular, the softer spectrum associated with the charm-quark contribution, combined with the intermediate size of its SM Yukawa coupling, makes this observable promising for extracting the charm Yukawa coupling. Additionally, it can be used to put bounds on the Yukawa couplings of the lighter quarks.

We further comment on the analytically resummed predictions in the right plot of figure 13. At NNLL+NLO accuracy, the spectra of the different flavour channels already exhibit different shapes, as observed here for N^{3}LL$'$ + aN^{3}LO results with a substantial reduction of the scale uncertainty. The uncertainties for the bottom-quark channel are noticeably larger compared to the other channels. In fact, the relative uncertainties for $b\bar{b} \to H$ at a given order are of similar size as those for $s\bar{s} \to H$ at one lower order. The main difference between the channels is the relative size of the PDF luminosities. As already pointed out in ref. [40] for $b\bar{b} \to H$, the $b\bar{b}$ Born channel is numerically suppressed by the small b-quark PDFs, the gluon-induced PDF channels, which start at one higher order, play a much more prominent role and explain the observed pattern of uncertainties for the different cases. We note that the $b\bar{b} \to H$ cross section in the right panel of figure 13 is only shown for $p_T > 4\,{\rm GeV}$, since with a bottom-quark mass of $m_b \sim 4.18\,{\rm GeV}$ the assumption of $m_q \ll p_T$, where the factorization theorem is valid, no longer applies for $p_T \lesssim 4\,{\rm GeV}$.

7.2 Simulations with diphoton signature in MiNNLO$_{\rm PS}$

In the MiNNLO$_{\rm PS}$ generator, the Higgs boson is treated as an on-shell asymptotic state. Its decay into photons can be modelled through Pythia8 using the zero-width approximation, assuming a branching ratio of BR($H \to \gamma\gamma$) = 0.227% [27]. Inspired by a fiducial region accessible by both the ATLAS and CMS detectors, we apply the following constraints on the rapidities and transverse momenta of the two photons:

$$|y(\gamma_i)| < 2.37, \quad \frac{p_T(\gamma_1)}{m(\gamma_1, \gamma_2)} > 0.35, \quad \frac{p_T(\gamma_2)}{m(\gamma_1, \gamma_2)} > 0.25\,. \tag{7.2}$$

---

[9]We note that the N^{3}LL$'$+aN^{3}LO spectra are normalised to the N^{3}LO cross sections obtained from `n3loxs` [168], which uses the results from refs. [8, 36]. The code was modified to obtain the N^{3}LO cross sections for $c\bar{c}H$ and $s\bar{s}H$.
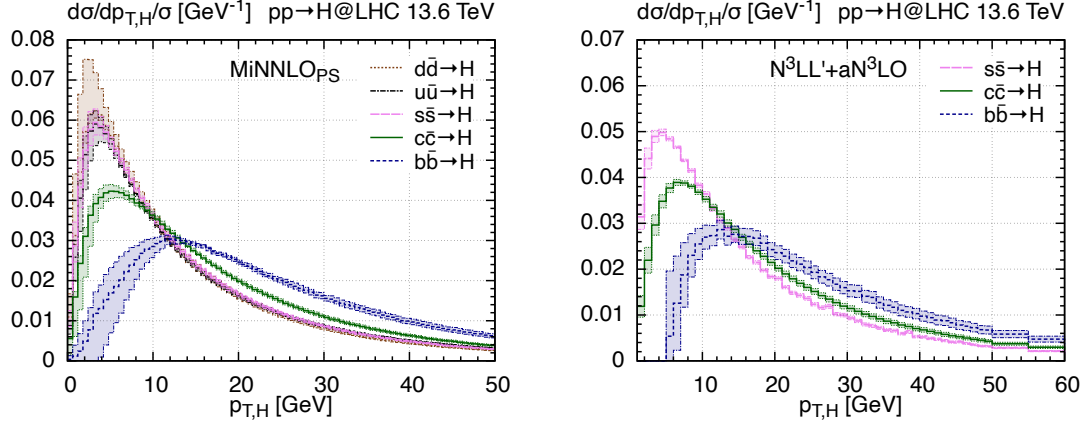
Figure 13: Transverse momentum spectra of the Higgs boson obtained with MiNNLO$_{\rm PS}$ (left) and at N^{3}LL$'$+aN^{3}LO (right) for the different quark-fusion channels: bottom (blue, dashed), charm (green, solid), strange (pink, long-dashed), and down (brown, dotted), and up (black, dotted-dashed). The distributions are normalised to their respective total cross sections.

Here, γ_1 denotes the hardest photon, i.e. the one with the largest transverse momentum. We employ the selection of eq. (7.2) as our fiducial selections and reconstruct the Higgs boson momentum from the photon pair.

To cross-check the MiNNLO$_{\rm PS}$ calculation with a fixed-order prediction, we have extended the public code SuSHi [169, 170], which computes the NNLO QCD cross section for $b\bar{b} \to H$ production, to support the light-quark fusion processes at NNLO in QCD. In table 7 we present the total inclusive cross section for the different light-quark Higgs boson production channels from SuSHi and MiNNLO$_{\rm PS}$ according using the setup in section 2. We recall that the values are obtained by assuming the bottom-quark Yukawa coupling in all production modes, as described in eq. (7.1), and must be rescaled by the ratio of appropriate squared Yukawa couplings to obtain the SM prediction.

We observe that the cross sections are enhanced by the respective quark PDF, with the light quarks receiving the strongest enhancement, which reduces as the quark mass increases. There is a good agreement between the fixed-order NNLO and MiNNLO$_{\rm PS}$ cross sections, particularly in the down- and up-quark channels. Scale uncertainties are significantly reduced for the lighter quark channels. Most notably bottom-quark fusion includes larger uncertainties due to the less accurate bottom PDFs, as discussed before.

In the last column of table 7 we report the integrated cross sections from the NNLO+PS simulation in the fiducial region defined in eq. (7.2). The three orders of magnitude difference compared to the fully inclusive case originates from the Higgs branching into photons. Among the initial-state quarks, the up quark shows the lowest efficiency in passing the fiducial selection, with only about 36% of diphoton events surviving the kinematical selections, compared to approximately 44% for the down quark and 59% for the charm quark.

Finally, we discuss the impact of the fiducial cuts on differential distributions of the Higgs

Flavour channel	SuSHi $\bar{\sigma}^{\text{inclusive}}_{q\bar{q}\to H}$	MiNNLO$_{\text{PS}}$ $\bar{\sigma}^{\text{inclusive}}_{q\bar{q}\to H}$	MiNNLO$_{\text{PS}}$ $\bar{\sigma}^{\text{fiducial}}_{q\bar{q}\to H\to\gamma\gamma}$
$d\bar{d}\to H$ $(y_d\to y_b)$	$11.46(9)^{+0.5\%}_{-1.1\%}$ pb	$11.442(3)^{+2.8\%}_{-2.4\%}$ pb	$11.420(5)^{+2.8\%}_{-2.4\%}$ fb
$u\bar{u}\to H$ $(y_u\to y_b)$	$16.46(1)^{+0.6\%}_{-1.1\%}$ pb	$16.182(5)^{+2.7\%}_{-2.3\%}$ pb	$13.169(8)^{+2.5\%}_{-2.1\%}$ fb
$s\bar{s}\to H$ $(y_s\to y_b)$	$4.454(3)^{+1.0\%}_{-1.4\%}$ pb	$4.676(1)^{+3.7\%}_{-1.8\%}$ pb	$6.215(3)^{+3.5\%}_{-1.7\%}$ fb
$c\bar{c}\to H$ $(y_c\to y_b)$	$1.849(1)^{+1.5\%}_{-2.9\%}$ pb	$1.778(6)^{+2.3\%}_{-0.9\%}$ pb	$2.399(1)^{+2.3\%}_{-1.0\%}$ fb
$b\bar{b}\to H$	$0.585(7)^{+7.0\%}_{-9.2\%}$ pb	$0.5757(4)^{+4.5\%}_{-8.0\%}$ pb	$0.8089(8)^{+4.7\%}_{-8.2\%}$ fb

Table 7: Comparison of SuSHi cross section numbers against the integrated MiNNLO$_{\text{PS}}$ results for Higgs boson production via light-quark fusion, with all Yukawa couplings set to the strength of the bottom-quark Yukawa. The last column presents the NNLO+PS results for $H\to\gamma\gamma$ production within the fiducial selection defined in eq. (7.2).
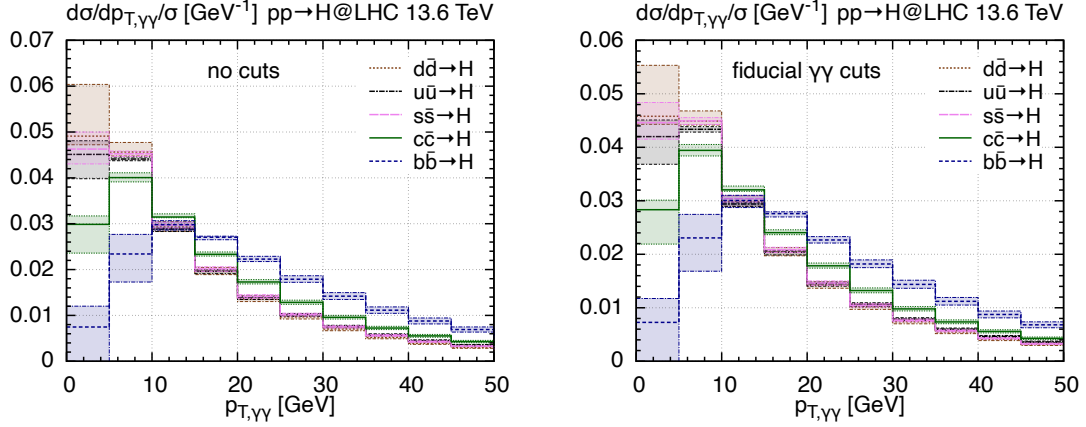
Figure 14: Transverse momentum spectra of the Higgs boson without kinematical selections (left) and within the fiducial region defined in eq. (7.2) (right) for the different quark-fusion channels: bottom (blue, dashed), charm (green, solid), strange (pink, long-dashed), and down (brown, dotted), and up (black, dotted-dashed). The distributions are normalised to their respective integrated cross sections.

boson in the various quark channels. In the left (right) plot of figure 14, we show the transverse momentum spectrum of the Higgs boson, reconstructed from the diphoton pair in the inclusive (fiducial) phase space. The distributions are normalised to their respective integrated cross sections. We observe that the shape of the different distributions changes relatively mildly when fiducial cuts on the photons are included. Moreover, the peak positions stay in the same place. As a result, extrapolations from the fiducial to the inclusive phase-space in experimental measurements should have a rather minor effect on the shape of the distribution.

We note that alternative channels sensitive to light-quark Yukawa couplings have been experimentally investigated recently, such as the reinterpretation of $WW\gamma$ analysis [171] and the Higgs decay rate into four leptons [172]. Novel approaches to probe the light-quark Yukawa couplings have also been discussed recently in refs. [173–175].

8 Conclusions

We have reported on new predictions for $b\bar{b}H$ production at the LHC at a centre-of-mass energy of 13.6 TeV. All cross sections are computed following the recommendations of the LHCHWG.

First, we have updated the predictions for the total inclusive cross section by interpolating the 13 TeV and 14 TeV cross section numbers from the 4FS and 5FS matched $\text{NLO+NNLL}_{\text{part}}+y_b y_t$ calculation. So far, the matching of the different flavour schemes has been performed only at the fully inclusive level for $b\bar{b}H$ production. Matched predictions of differential state-of-the-art $b\bar{b}H$ predictions in 4FS and 5FS could, in principle, be obtained by extending differential matching approaches, such as those discussed in refs. [176, 177], to higher orders.

As far as differential calculations for $b\bar{b}H$ production are concerned, this report focusses on new state-of-the-art predictions in either scheme. Specifically, novel results for the Higgs transverse momentum distribution have been discussed based on the analytic resummation at $\text{N}^3\text{LL}' + \text{aN}^3\text{LO}$ accuracy. In the future, this calculation could be extended by the matching with the exact N^3LO corrections for Higgs boson production via bottom-quark fusion.

We then presented the first numerical comparison of the recently developed $\text{MiNNLO}_{\text{PS}}$ and GENEVA generators for $b\bar{b}H$ production in the massless scheme (i.e. the $b\bar{b} \to H$ process) at NNLO+PS accuracy. We find their predictions to be compatible within the respective theoretical uncertainties for the observables studied, showing good agreement also with the analytically resummed result for the Higgs transverse momentum spectrum. We also included a proof-of-concept study of the $\text{MiNNLO}_{\text{PS}}$ generator for BSM applications involving heavy-Higgs boson production with an enhanced bottom-quark Yukawa coupling, considering a specific MSSM scenario for a still allowed parameter setting.

Also the NNLO corrections to $b\bar{b}H$ production in the massive scheme have recently been computed, including parton shower matching, in the $\text{MiNNLO}_{\text{PS}}$ framework. We have studied the sizeable NNLO effects, and we compared 4FS and 5FS $\text{MiNNLO}_{\text{PS}}$ predictions. For the first time, 4FS and 5FS predictions are finally in full agreement, when the cross section in both schemes is computed to NNLO in QCD. Thus, the inclusion of NNLO corrections in the massive scheme, finally resolves the long-standing 4FS–5FS discrepancy and discussion about the *appropriate* flavour scheme for the $b\bar{b}H$ process. As a result, the corresponding theoretical uncertainty in the modelling of the $b\bar{b}H$ signal cross section is substantially reduced.

Apart from single-Higgs boson production, the $b\bar{b}H$ process is an important background to HH searches in all channels involving at least one Higgs boson decaying into two bottom quarks. We have discussed the impact of 4FS predictions in the fiducial phase-space region relevant for HH studies. For the y_b^2 contribution, we have employed the previously introduced $\text{MiNNLO}_{\text{PS}}$ generator. Also in this case, the inclusion of the NNLO QCD corrections leads to a strong reduction of the scale uncertainties. The y_t^2 contribution, on the other hand, which is even larger than the y_b^2 one, is modelled from the NLO+PS generator developed within MAD-

GRAPH5_AMC@NLO. So far, the y_t^2 contribution was modelled in the 5FS by selecting events from the NNLOPS generator for inclusive Higgs boson production in gluon fusion, which is effectively only LO accurate for $b\bar{b}H$ final state, and was assigned with a 100% uncertainty. Since also Higgs plus light jet contributions can enter the HH selection through mistagging, we have suggested a consistent approach within the 4FS to combine those contributions from NNLOPS generator (removing all $b\bar{b}H$ final states) with the more accurate NLO+PS calculation for $b\bar{b}H$ production. As an important outlook for HH studies, the y_t^2 $b\bar{b}H$ component in the HTL approximation could in the future be obtained at NNLO+PS using the existing MiNNLO$_{\rm PS}$ framework, with the main limitation being the absence of the required two-loop amplitudes. Moreover, the NLO calculation of the y_t^2 $b\bar{b}H$ contribution beyond the HTL approximation, which requires the corresponding exact two-loop virtual amplitude, would be highly valuable to further reduce the theoretical uncertainty.

In the last section of the report, we have discussed light-quark Yukawa contributions to Higgs-boson production. The production mechanism corresponds exactly to the one of $b\bar{b}H$ production in the massless scheme, i.e. $q\bar{q} \to H$. We find that the shape of the transverse momentum spectrum is very sensitive to the different initial state quarks, due to PDF effects. We have also considered $q\bar{q} \to H$ production with the Higgs decaying into two photons, making use of the possibility to decay the Higgs boson through PYTHIA8 within the MiNNLO$_{\rm PS}$ generator. To further improve the theoretical modeling of $c\bar{c}H$ final states, which can be important to extract the charm-quark Yukawa coupling, the NNLO(+PS) calculation of $c\bar{c}H$ production in the massive scheme (i.e. a three flavour scheme) could be considered within the MiNNLO$_{\rm PS}$ framework.

Citation policy. The present work consists of contributions from different collaborations. If some of the results are employed for scientific publications, together with this work, one should cite the corresponding work in refs. [4, 16, 17, 22, 23, 40, 162].

Data Availability Statement. All data used to produce the plots are available upon request by contacting the LHCHWG bbH/bH theory conveners via email.

Acknowledgements. This work has been carried out within the LHCHWG, as a contribution to the Yellow Report 5. We thank all the Working Group 3 conveners for coordinating the activities, in particular Tatjana Lenz. CB is grateful to Tommaso Giani and Jan Lukas Späh for discussions on Yukawa interactions via light-quark fusion. We have used the Max Planck Computing and Data Facility (MPCDF) in Garching to carry out the MiNNLO$_{\rm PS}$ simulations presented here. AG, RvK and FK have received funding from the European Research Council (ERC) under the European Union's Horizon 2020 research and innovation programme (Grant agreement 101002090 COLORFREE). MZ acknowledges the financial support by the MUR (Italy), with funds of the European Union (NextGenerationEU), through the PRIN2022 grant 2022EZ3S3F.

References

[1] CMS collaboration, A. Hayrapetyan et al., *Search for bottom quark associated production of the standard model Higgs boson in final states with leptons in proton-proton collisions at s=13TeV*, *Phys. Lett. B* **860** (2025) 139173, [2408.01344].

[2] S. Dittmaier, M. Krämer and M. Spira, *Higgs radiation off bottom quarks at the Tevatron and the CERN LHC*, *Phys.Rev.* **D70** (2004) 074010, [hep-ph/0309204].

[3] S. Dawson, C. Jackson, L. Reina and D. Wackeroth, *Exclusive Higgs boson production with bottom quarks at hadron colliders*, *Phys.Rev.* **D69** (2004) 074027, [hep-ph/0311067].

[4] C. Biello, J. Mazzitelli, A. Sankar, M. Wiesemann and G. Zanderighi, *Higgs boson production in association with massive bottom quarks at NNLO+PS*, 2412.09510.

[5] D. Dicus, T. Stelzer, Z. Sullivan and S. Willenbrock, *Higgs boson production in association with bottom quarks at next-to-leading order*, *Phys.Rev.* **D59** (1999) 094016, [hep-ph/9811492].

[6] C. Balazs and C. Yuan, *Higgs boson production at hadron colliders with soft gluon effects. 1. Backgrounds*, *Phys. Rev.* **D59** (1999) 114007, [hep-ph/9810319].

[7] R. V. Harlander and W. B. Kilgore, *Higgs boson production in bottom quark fusion at next-to-next-to-leading order*, *Physical Review D* **68** (July, 2003) .

[8] C. Duhr, F. Dulat and B. Mistlberger, *Higgs Boson Production in Bottom-Quark Fusion to Third Order in the Strong Coupling*, *Phys. Rev. Lett.* **125** (2020) 051804, [1904.09990].

[9] J. Campbell, S. Dawson, S. Dittmaier, C. Jackson, M. Kramer, F. Maltoni et al., *Higgs Boson Production in Association with Bottom Quarks*, in *Physics at TeV colliders. Proceedings, Workshop, Les Houches.*, pp. 2–8, 2003. 0405302.

[10] F. Maltoni, G. Ridolfi and M. Ubiali, *b-initiated processes at the LHC: a reappraisal*, *JHEP* **07** (2012) 022, [1203.6393].

[11] R. Harlander, M. Krämer and M. Schumacher, *Bottom-quark associated Higgs-boson production: reconciling the four- and five-flavour scheme approach*, 2011.

[12] S. Forte, D. Napoletano and M. Ubiali, *Higgs production in bottom-quark fusion in a matched scheme*, *Phys. Lett.* **B751** (2015) 331–337, [1508.01529].

[13] S. Forte, D. Napoletano and M. Ubiali, *Higgs production in bottom-quark fusion: matching beyond leading order*, *Phys. Lett.* **B763** (2016) 190–196, [1607.00389].

[14] M. Bonvini, A. S. Papanastasiou and F. J. Tackmann, *Resummation and matching of b-quark mass effects in $b\bar{b}H$ production*, *JHEP* **11** (2015) 196, [1508.03288].

[15] M. Bonvini, A. S. Papanastasiou and F. J. Tackmann, *Matched predictions for the $b\bar{b}H$ cross section at the 13 TeV LHC*, *JHEP* **10** (2016) 053, [1605.01733].

[16] A. Gavardi, R. von Kuk and M. A. Lim, *Resumming transverse observables for NNLO+PS matching in GENEVA*, 2505.14773.

[17] C. Biello, A. Sankar, M. Wiesemann and G. Zanderighi, *NNLO+PS predictions for Higgs production through bottom-quark annihilation with MINNLO$_{PS}$*, *Eur. Phys. J. C* **84** (2024) 479, [2402.04025].

[18] K. Hamilton, P. Nason, C. Oleari and G. Zanderighi, *Merging H/W/Z + 0 and 1 jet at NLO with no merging scale: a path to parton shower + NNLO matching*, *JHEP* **05** (2013) 082, [1212.4504].

[19] K. Hamilton, P. Nason, E. Re and G. Zanderighi, *NNLOPS simulation of Higgs boson production*, *JHEP* **10** (2013) 222, [1309.0017].

[20] K. Hamilton, P. Nason and G. Zanderighi, *Finite quark-mass effects in the NNLOPS POWHEG+MiNLO Higgs generator*, *JHEP* **05** (2015) 140, [1501.04637].

[21] S. Dawson, C. B. Jackson, L. Reina and D. Wackeroth, *Higgs boson production with one bottom quark jet at hadron colliders*, *Phys. Rev. Lett.* **94** (2005) 031802, [hep-ph/0408077].

[22] N. Deutschmann, F. Maltoni, M. Wiesemann and M. Zaro, *Top-Yukawa contributions to bbH production at the LHC*, *JHEP* **07** (2019) 054, [1808.01660].

[23] S. Manzoni, E. Mazzeo, J. Mazzitelli, M. Wiesemann and M. Zaro, *Taming a leading theoretical uncertainty in HH measurements via accurate simulations for $b\bar{b}H$ production*, *JHEP* **09** (2023) 179, [2307.09992].

[24] Y. Zhang, *NLO electroweak effects on the Higgs boson production in association with a bottom quark pair at the LHC*, *Phys. Rev. D* **96** (2017) 113009, [1708.08790].

[25] D. Pagani, H.-S. Shao and M. Zaro, *RIP $Hb\bar{b}$: how other Higgs production modes conspire to kill a rare signal at the LHC*, *JHEP* **11** (2020) 036, [2005.10277].

[26] C. Grojean, A. Paul and Z. Qian, *Resurrecting $b\bar{b}h$ with kinematic shapes*, *JHEP* **04** (2021) 139, [2011.13945].

[27] LHC HIGGS CROSS SECTION WORKING GROUP collaboration, D. de Florian et al., *Handbook of LHC Higgs Cross Sections: 4. Deciphering the Nature of the Higgs Sector*, 1610.07922.

[28] PDF4LHC WORKING GROUP collaboration, R. D. Ball et al., *The PDF4LHC21 combination of global PDF fits for the LHC Run III*, *J. Phys. G* **49** (2022) 080501, [2203.05506].

[29] A. Buckley, J. Ferrando, S. Lloyd, K. Nordström, B. Page, M. Rüfenacht et al., *LHAPDF6: parton density access in the LHC precision era*, *Eur. Phys. J.* **C75** (2015) 132, [1412.7420].

[30] A. Karlberg et al., *Ad interim recommendations for the Higgs boson production cross sections at $\sqrt{s} = 13.6$ TeV*, 2402.09955.

[31] PARTICLE DATA GROUP collaboration, S. Navas et al., *Review of particle physics*, *Phys. Rev. D* **110** (2024) 030001.

[32] R. V. Harlander and W. B. Kilgore, *Next-to-next-to-leading order Higgs production at hadron colliders*, *Phys.Rev.Lett.* **88** (2002) 201801, [hep-ph/0201206].

[33] P. A. Baikov, K. G. Chetyrkin and J. H. Kühn, *Quark mass and field anomalous dimensions to $\mathcal{O}\left(\alpha_s^5\right)$*, *Journal of High Energy Physics* **2014** (Oct., 2014) .

[34] A. Vogt, *Efficient evolution of unpolarized and polarized parton distributions with QCD-PEGASUS*, *Comput. Phys. Commun.* **170** (2005) 65–92, [hep-ph/0408244].

[35] M. Wiesemann, R. Frederix, S. Frixione, V. Hirschi, F. Maltoni and P. Torrielli, *Higgs production in association with bottom quarks*, *JHEP* **02** (2015) 132, [1409.5301].

[36] C. Duhr, F. Dulat, V. Hirschi and B. Mistlberger, *Higgs production in bottom quark fusion: matching the 4- and 5-flavour schemes to third order in the strong coupling*, *JHEP* **08** (2020) 017, [2004.04752].

[37] M. A. Ebert, S. Liebler, I. Moult, I. W. Stewart, F. J. Tackmann, K. Tackmann et al., *Exploiting jet binning to identify the initial state of high-mass resonances*, *Phys. Rev. D* **94** (2016) 051901, [1605.06114].

[38] F. Bishara, U. Haisch, P. F. Monni and E. Re, *Constraining light-quark Yukawa couplings from Higgs distributions*, *Phys. Rev. Lett.* **118** (2017) 121801, [1606.09253].

[39] Y. Soreq, H. X. Zhu and J. Zupan, *Light quark Yukawa couplings from Higgs kinematics*, *JHEP* **12** (2016) 045, [1606.09621].

[40] P. Cal, R. von Kuk, M. A. Lim and F. J. Tackmann, *qT spectrum for Higgs boson production via heavy quark annihilation at N3LL'+aN3LO*, *Phys. Rev. D* **110** (2024) 076005, [2306.16458].

[41] C. F. Berger, C. Marcantonini, I. W. Stewart, F. J. Tackmann and W. J. Waalewijn, *Higgs Production with a Central Jet Veto at NNLL+NNLO*, *JHEP* **04** (2011) 092, [1012.4480].

[42] R. V. Harlander, A. Tripathi and M. Wiesemann, *Higgs production in bottom quark annihilation: Transverse momentum distribution at NNLO+NNLL*, *Phys. Rev.* **D90** (2014) 015017, [1403.7196].

[43] J. C. Collins and D. E. Soper, *Back-To-Back Jets in QCD*, *Nucl. Phys.* **B193** (1981) 381.

[44] J. C. Collins and D. E. Soper, *Back-To-Back Jets: Fourier Transform from B to K-Transverse*, *Nucl. Phys. B* **197** (1982) 446–476.

[45] J. C. Collins, D. E. Soper and G. F. Sterman, *Transverse Momentum Distribution in Drell-Yan Pair and W and Z Boson Production*, *Nucl. Phys.* **B250** (1985) 199–224.

[46] C. W. Bauer, S. Fleming, D. Pirjol and I. W. Stewart, *An Effective field theory for collinear and soft gluons: Heavy to light decays*, *Phys.Rev.* **D63** (2001) 114020, [hep-ph/0011336].

[47] C. W. Bauer and I. W. Stewart, *Invariant operators in collinear effective theory*, *Phys. Lett. B* **516** (2001) 134–142, [hep-ph/0107001].

[48] C. W. Bauer, D. Pirjol and I. W. Stewart, *Soft collinear factorization in effective field theory*, *Phys.Rev.* **D65** (2002) 054022, [hep-ph/0109045].

[49] C. W. Bauer, S. Fleming, D. Pirjol, I. Z. Rothstein and I. W. Stewart, *Hard scattering factorization from effective field theory*, *Phys. Rev. D* **66** (2002) 014017, [hep-ph/0202088].

[50] M. Beneke, A. P. Chapovsky, M. Diehl and T. Feldmann, *Soft collinear effective theory and heavy to light currents beyond leading power*, *Nucl. Phys. B* **643** (2002) 431–476, [hep-ph/0206152].

[51] J.-Y. Chiu, A. Jain, D. Neill and I. Z. Rothstein, *A Formalism for the Systematic Treatment of Rapidity Logarithms in Quantum Field Theory*, *JHEP* **05** (2012) 084, [1202.0814].

[52] Y. Li, D. Neill and H. X. Zhu, *An exponential regulator for rapidity divergences*, *Nucl. Phys. B* **960** (2020) 115193, [1604.00392].

[53] M. A. Ebert and F. J. Tackmann, *Resummation of transverse momentum distributions in distribution space*, *JHEP* **02** (2017) 110, [1611.08610].

[54] M. A. Ebert, J. K. L. Michel, I. W. Stewart and F. J. Tackmann, *Drell-Yan q_T resummation of fiducial power corrections at N^3LL*, *JHEP* **04** (2021) 102, [2006.11382].

[55] T. Gehrmann and D. Kara, *The $Hb\bar{b}$ form factor to three loops in QCD*, *JHEP* **09** (2014) 174, [1407.8114].

[56] M. A. Ebert, J. K. L. Michel and F. J. Tackmann, *Resummation Improved Rapidity Spectrum for Gluon Fusion Higgs Production*, 1702.00794.

[57] T. Lübbert, J. Oredsson and M. Stahlhofen, *Rapidity renormalized TMD soft and beam functions at two loops*, *JHEP* **03** (2016) 168, [1602.01829].

[58] Y. Li and H. X. Zhu, *Bootstrapping rapidity anomalous dimensions for transverse-momentum resummation*, *Phys. Rev. Lett.* **118** (2017) 022004, [1604.01404].

[59] G. Billis, M. A. Ebert, J. K. L. Michel and F. J. Tackmann, *A toolbox for q_T and 0-jettiness subtractions at N^3LO*, *Eur. Phys. J. Plus* **136** (2021) 214, [1909.00811].

[60] M.-x. Luo, T.-Z. Yang, H. X. Zhu and Y. J. Zhu, *Quark Transverse Parton Distribution at the Next-to-Next-to-Next-to-Leading Order*, *Phys. Rev. Lett.* **124** (2020) 092001, [1912.05778].

[61] M. A. Ebert, B. Mistlberger and G. Vita, *Transverse momentum dependent PDFs at N^3LO*, *JHEP* **09** (2020) 146, [2006.05329].

[62] S. Moch, J. A. M. Vermaseren and A. Vogt, *The Quark form-factor at higher orders*, *JHEP* **08** (2005) 049, [hep-ph/0507039].

[63] I. W. Stewart, F. J. Tackmann and W. J. Waalewijn, *The Quark Beam Function at NNLL*, *JHEP* **09** (2010) 005, [1002.2213].

[64] R. Brüser, Z. L. Liu and M. Stahlhofen, *Three-Loop Quark Jet Function*, *Phys. Rev. Lett.* **121** (2018) 072003, [1804.09722].

[65] A. A. Vladimirov, *Correspondence between soft and rapidity anomalous dimensions*, *Phys. Rev. Lett.* **118** (2017) 062001, [1610.05791].

[66] G. P. Korchemsky and A. V. Radyushkin, *Renormalization of the Wilson Loops Beyond the Leading Order*, *Nucl. Phys. B* **283** (1987) 342–364.

[67] S. Moch, J. A. M. Vermaseren and A. Vogt, *The three-loop splitting functions in QCD: The nonsinglet case*, *Nucl. Phys.* **B688** (2004) 101–134, [hep-ph/0403192].

[68] R. Brüser, A. Grozin, J. M. Henn and M. Stahlhofen, *Matter dependence of the four-loop QCD cusp anomalous dimension: from small angles to all angles*, *JHEP* **05** (2019) 186, [1902.05076].

[69] J. M. Henn, G. P. Korchemsky and B. Mistlberger, *The full four-loop cusp anomalous dimension in $\mathcal{N} = 4$ super Yang-Mills and QCD*, *JHEP* **04** (2020) 018, [1911.10174].

[70] A. von Manteuffel, E. Panzer and R. M. Schabinger, *Analytic four-loop anomalous dimensions in massless QCD from form factors*, *Phys. Rev. Lett.* **124** (2020) 162001, [2002.04617].

[71] O. V. Tarasov, A. A. Vladimirov and A. Y. Zharkov, *The Gell-Mann-Low Function of QCD in the Three Loop Approximation*, *Phys. Lett. B* **93** (1980) 429–432.

[72] S. A. Larin and J. A. M. Vermaseren, *The Three loop QCD Beta function and anomalous dimensions*, *Phys. Lett. B* **303** (1993) 334–336, [hep-ph/9302208].

[73] T. van Ritbergen, J. A. M. Vermaseren and S. A. Larin, *The Four loop beta function in quantum chromodynamics*, *Phys. Lett.* **B400** (1997) 379–384, [hep-ph/9701390].

[74] M. Czakon, *The Four-loop QCD beta-function and anomalous dimensions*, *Nucl. Phys.* **B710** (2005) 485–498, [hep-ph/0411261].

[75] B. Dehnadi, I. Novikov and F. J. Tackmann, *The photon energy spectrum in $B \to X_s\gamma$ at N^3LL'*, *JHEP* **07** (2023) 214, [2211.07663].

[76] M. A. Ebert, J. K. L. Michel, F. J. Tackmann et al., *SCETlib: A C++ Package for Numerical Calculations in QCD and Soft-Collinear Effective Theory*, *DESY-17-099* (2018) .

[77] P. F. Monni, P. Nason, E. Re, M. Wiesemann and G. Zanderighi, *MiNNLO$_{PS}$: a new method to match NNLO QCD to parton showers*, *JHEP* **05** (2020) 143, [1908.06987].

[78] P. F. Monni, E. Re and M. Wiesemann, *MiNNLO$_{PS}$: optimizing $2 \to 1$ hadronic processes*, *Eur. Phys. J. C* **80** (2020) 1075, [2006.04133].

[79] S. Alioli, C. W. Bauer, C. J. Berggren, A. Hornig, F. J. Tackmann, C. K. Vermilion et al., *Combining Higher-Order Resummation with Multiple NLO Calculations and Parton Showers in GENEVA*, *JHEP* **09** (2013) 120, [1211.7049].

[80] S. Alioli, C. W. Bauer, C. Berggren, F. J. Tackmann, J. R. Walsh and S. Zuberi, *Matching Fully Differential NNLO Calculations and Parton Showers*, *JHEP* **06** (2014) 089, [1311.0286].

[81] S. Alioli, C. W. Bauer, A. Broggio, A. Gavardi, S. Kallweit, M. A. Lim et al., *Matching NNLO predictions to parton showers using N3LL color-singlet transverse momentum resummation in geneva*, *Phys. Rev. D* **104** (2021) 094020, [2102.08390].

[82] A. Gavardi, M. A. Lim, S. Alioli and F. Tackmann, *NNLO+PS W^+W^- production using jet veto resummation at NNLL'*, 2308.11577.

[83] M. Ebert, L. Rottoli, M. Wiesemann, G. Zanderighi and S. Zanoli, *Jettiness formulation of the MiNNLO$_{PS}$ method*, *JHEP* **07** (2024) 085, [2402.00596].

[84] D. Lombardi, M. Wiesemann and G. Zanderighi, *Advancing MiNNLO$_{PS}$ to diboson processes: $Z\gamma$ production at NNLO+PS*, *JHEP* **06** (2021) 095, [2010.10478].

[85] D. Lombardi, M. Wiesemann and G. Zanderighi, *WW production at NNLO+PS with MiNNLO$_{PS}$*, *JHEP* **11** (2021) 230, [2103.12077].

[86] L. Buonocore, G. Koole, D. Lombardi, L. Rottoli, M. Wiesemann and G. Zanderighi, *ZZ production at nNNLO+PS with MiNNLO$_{PS}$*, *JHEP* **01** (2022) 072, [2108.05337].

[87] D. Lombardi, M. Wiesemann and G. Zanderighi, *Anomalous couplings in $Z\gamma$ events at NNLO+PS and improving $\nu\bar{\nu}\gamma$ backgrounds in dark-matter searches*, *Phys. Lett. B* **824** (2022) 136846, [2108.11315].

[88] S. Zanoli, M. Chiesa, E. Re, M. Wiesemann and G. Zanderighi, *Next-to-next-to-leading order event generation for VH production with $H \to b\bar{b}$ decay*, 2112.04168.

[89] A. Gavardi, C. Oleari and E. Re, *NNLO+PS Monte Carlo simulation of photon pair production with MiNNLO$_{PS}$*, *JHEP* **09** (2022) 061, [2204.12602].

[90] U. Haisch, D. J. Scott, M. Wiesemann, G. Zanderighi and S. Zanoli, *NNLO event generation for $pp \to Zh \to \ell^+\ell^- b\bar{b}$ production in the SM effective field theory*, *JHEP* **07** (2022) 054, [2204.00663].

[91] J. M. Lindert, D. Lombardi, M. Wiesemann, G. Zanderighi and S. Zanoli, *$W^\pm Z$ production at NNLO QCD and NLO EW matched to parton showers with MiNNLO$_{PS}$*, *JHEP* **11** (2022) 036, [2208.12660].

[92] M. Niggetiedt and M. Wiesemann, *Higgs-boson production in the full theory at NNLO+PS*, *Phys. Lett. B* **858** (2024) 139043, [2407.01354].

[93] S. Alioli, C. W. Bauer, C. Berggren, F. J. Tackmann and J. R. Walsh, *Drell-Yan production at NNLL'+NNLO matched to parton showers*, *Phys. Rev.* **D92** (2015) 094020, [1508.01475].

[94] S. Alioli, A. Broggio, S. Kallweit, M. A. Lim and L. Rottoli, *Higgsstrahlung at NNLL prime+NNLO matched to parton showers in GENEVA*, *Phys. Rev. D* **100** (2019) 096016, [1909.02026].

[95] S. Alioli, A. Broggio, A. Gavardi, S. Kallweit, M. A. Lim, R. Nagar et al., *Precise predictions for photon pair production matched to parton showers in GENEVA*, *JHEP* **04** (2021) 041, [2010.10498].

[96] S. Alioli, A. Broggio, A. Gavardi, S. Kallweit, M. A. Lim, R. Nagar et al., *Next-to-next-to-leading order event generation for Z boson pair production matched to parton shower*, *Phys. Lett. B* **818** (2021) 136380, [2103.01214].

[97] S. Alioli, G. Billis, A. Broggio, A. Gavardi, S. Kallweit, M. A. Lim et al., *Double Higgs production at NNLO interfaced to parton showers in GENEVA*, *JHEP* **06** (2023) 205, [2212.10489].

[98] S. Alioli, G. Billis, A. Broggio, A. Gavardi, S. Kallweit, M. A. Lim et al., *Refining the GENEVA method for Higgs boson production via gluon fusion*, *JHEP* **05** (2023) 128, [2301.11875].

[99] S. Alioli, G. Marinelli and D. Napoletano, *NNLO+PS Double Higgs boson production with top-quark mass corrections in GENEVA*, 2507.08558.

[100] J. Mazzitelli, P. F. Monni, P. Nason, E. Re, M. Wiesemann and G. Zanderighi, *Next-to-Next-to-Leading Order Event Generation for Top-Quark Pair Production*, *Phys. Rev. Lett.* **127** (2021) 062001, [2012.14267].

[101] J. Mazzitelli, P. F. Monni, P. Nason, E. Re, M. Wiesemann and G. Zanderighi, *Top-pair production at the LHC with MINNLO$_{PS}$*, *JHEP* **04** (2022) 079, [2112.12135].

[102] J. Mazzitelli, A. Ratti, M. Wiesemann and G. Zanderighi, *B-hadron production at the LHC from bottom-quark pair production at NNLO+PS*, *Phys. Lett. B* **843** (2023) 137991, [2302.01645].

[103] J. Mazzitelli, V. Sotnikov and M. Wiesemann, *Next-to-next-to-leading order event generation for Z-boson production in association with a bottom-quark pair*, 2404.08598.

[104] S. Frixione, P. Nason and C. Oleari, *Matching NLO QCD computations with Parton Shower simulations: the POWHEG method*, *JHEP* **11** (2007) 070, [0709.2092].

[105] S. Alioli, P. Nason, C. Oleari and E. Re, *A general framework for implementing NLO calculations in shower Monte Carlo programs: the POWHEG BOX*, *JHEP* **06** (2010) 043, [1002.2581].

[106] K. Hamilton, P. Nason and G. Zanderighi, *MINLO: Multi-Scale Improved NLO*, *JHEP* **10** (2012) 155, [1206.3572].

[107] P. Fayet, *Supergauge Invariant Extension of the Higgs Mechanism and a Model for the electron and Its Neutrino*, *Nucl. Phys. B* **90** (1975) 104–124.

[108] P. Fayet, *Supersymmetry and Weak, Electromagnetic and Strong Interactions*, *Phys. Lett. B* **64** (1976) 159.

[109] P. Fayet, *Spontaneously Broken Supersymmetric Theories of Weak, Electromagnetic and Strong Interactions*, *Phys. Lett. B* **69** (1977) 489.

[110] B. A. Ovrut, *Supersymmetry, supergravity, and particle physics*, *AIP Conf. Proc.* **143** (1986) 97–121.

[111] H. E. Haber and G. L. Kane, *The Search for Supersymmetry: Probing Physics Beyond the Standard Model*, *Phys. Rept.* **117** (1985) 75–263.

[112] J. F. Gunion and H. E. Haber, *Higgs Bosons in Supersymmetric Models. 1.*, *Nucl. Phys. B* **272** (1986) 1.

[113] G. C. Branco, P. M. Ferreira, L. Lavoura, M. N. Rebelo, M. Sher and J. P. Silva, *Theory and phenomenology of two-Higgs-doublet models*, *Phys. Rept.* **516** (2012) 1–102, [1106.0034].

[114] P. Slavich et al., *Higgs-mass predictions in the MSSM and beyond*, *Eur. Phys. J. C* **81** (2021) 450, [2012.15629].

[115] E. Bagnaschi et al., *MSSM Higgs Boson Searches at the LHC: Benchmark Scenarios for Run 2 and Beyond*, *Eur. Phys. J. C* **79** (2019) 617, [1808.07542].

[116] S. Dittmaier, P. Häfliger, M. Krämer, M. Spira and M. Walser, *Neutral MSSM Higgs-boson*

production with heavy quarks: NLO supersymmetric QCD corrections, *Phys. Rev. D* **90** (2014) 035010, [1406.5307].

[117] T. Banks, *Supersymmetry and the Quark Mass Matrix*, *Nucl. Phys. B* **303** (1988) 172–188.

[118] L. J. Hall, R. Rattazzi and U. Sarid, *The Top quark mass in supersymmetric SO(10) unification*, *Phys. Rev. D* **50** (1994) 7048–7065, [hep-ph/9306309].

[119] M. Carena, M. Olechowski, S. Pokorski and C. E. M. Wagner, *Electroweak symmetry breaking and bottom - top Yukawa unification*, *Nucl. Phys. B* **426** (1994) 269–300, [hep-ph/9402253].

[120] M. Carena, D. Garcia, U. Nierste and C. E. M. Wagner, *b → sγ and supersymmetry with large* tan β, *Phys. Lett. B* **499** (2001) 141–146, [hep-ph/0010003].

[121] J. Guasch, P. Hafliger and M. Spira, *MSSM Higgs decays to bottom quark pairs revisited*, *Phys. Rev. D* **68** (2003) 115001, [hep-ph/0305101].

[122] D. Noth and M. Spira, *Higgs Boson Couplings to Bottom Quarks: Two-Loop Supersymmetry-QCD Corrections*, *Phys. Rev. Lett.* **101** (2008) 181801, [0808.0087].

[123] D. Noth and M. Spira, *Supersymmetric Higgs Yukawa Couplings to Bottom Quarks at next-to-next-to-leading Order*, *JHEP* **06** (2011) 084, [1001.1935].

[124] L. Mihaila and C. Reisser, $\mathcal{O}(\alpha_s^2)$ *corrections to fermionic Higgs decays in the MSSM*, *JHEP* **08** (2010) 021, [1007.0693].

[125] A. Crivellin and C. Greub, *Two-loop supersymmetric QCD corrections to Higgs-quark-quark couplings in the generic MSSM*, *Phys. Rev. D* **87** (2013) 015013, [1210.7453].

[126] M. Ghezzi, S. Glaus, D. Müller, T. Schmidt and M. Spira, *Refinements of the Bottom and Strange MSSM Higgs Yukawa Couplings at NNLO*, *Eur. Phys. J. C* **81** (2021) 259, [1711.02555].

[127] A. Djouadi, J. Kalinowski and M. Spira, *HDECAY: A Program for Higgs boson decays in the standard model and its supersymmetric extension*, *Comput. Phys. Commun.* **108** (1998) 56–74, [hep-ph/9704448].

[128] HDECAY collaboration, A. Djouadi, J. Kalinowski, M. Muehlleitner and M. Spira, *HDECAY: Twenty++ years after*, *Comput. Phys. Commun.* **238** (2019) 214–231, [1801.09506].

[129] H. X. Zhu, C. S. Li, H. T. Li, D. Y. Shao and L. L. Yang, *Transverse-momentum resummation for top-quark pairs at hadron colliders*, *Phys. Rev. Lett.* **110** (2013) 082001, [1208.5774].

[130] H. T. Li, C. S. Li, D. Y. Shao, L. L. Yang and H. X. Zhu, *Top quark pair production at small transverse momentum in hadronic collisions*, *Phys. Rev. D* **88** (2013) 074004, [1307.2464].

[131] S. Catani, M. Grazzini and A. Torre, *Transverse-momentum resummation for heavy-quark hadroproduction*, *Nucl. Phys.* **B890** (2014) 518–538, [1408.4564].

[132] S. Catani, M. Grazzini and H. Sargsyan, *Transverse-momentum resummation for top-quark pair production at the LHC*, *JHEP* **11** (2018) 061, [1806.01601].

[133] S. Catani and M. Grazzini, *QCD transverse-momentum resummation in gluon fusion processes*, *Nucl. Phys.* **B845** (2011) 297–323, [1011.3918].

[134] G. Bozzi, S. Catani, D. de Florian and M. Grazzini, *Transverse-momentum resummation and the spectrum of the Higgs boson at the LHC*, *Nucl. Phys.* **B737** (2006) 73–120, [hep-ph/0508068].

[135] A. Mitov and S. Moch, *The Singular behavior of massive QCD amplitudes*, *JHEP* **05** (2007) 001, [hep-ph/0612149].

[136] G. Wang, T. Xia, L. L. Yang and X. Ye, *On the high-energy behavior of massive QCD amplitudes*, *JHEP* **05** (2024) 082, [2312.12242].

[137] S. Badger, H. B. Hartanto, R. Poncelet, Z. Wu, Y. Zhang and S. Zoia, *Full-colour double-virtual amplitudes for associated production of a Higgs boson with a bottom-quark pair at the LHC*, *JHEP* **03** (2025) 066, [2412.06519].

[138] S. Badger, H. B. Hartanto, J. Kryś and S. Zoia, *Two-loop leading-colour QCD helicity amplitudes for Higgs boson production in association with a bottom-quark pair at the LHC*, *JHEP* **11** (2021) 012, [2107.14733].

[139] F. Caola, R. Grabarczyk, M. L. Hutt, G. P. Salam, L. Scyboz and J. Thaler, *Flavored jets with exact anti-kt kinematics and tests of infrared and collinear safety*, *Phys. Rev. D* **108** (2023) 094010, [2306.07314].

[140] ATLAS Collaboration, *Combination of Searches for Higgs Boson Pair Production in pp Collisions at $\sqrt{s} = 13\,TeV$ with the ATLAS detector*, *Phys. Rev. Lett.* **133** (2024) 101801, [2406.09971].

[141] CMS Collaboration, *A portrait of the Higgs boson by the CMS experiment ten years after the discovery*, *Nature* **607** (2022) 60–68, [2207.00043].

[142] C. Bierlich et al., *A comprehensive guide to the physics and usage of PYTHIA 8.3*, *SciPost Phys. Codeb.* **2022** (2022) 8, [2203.11601].

[143] J. Alwall, R. Frederix, S. Frixione, V. Hirschi, F. Maltoni, O. Mattelaer et al., *The automated computation of tree-level and next-to-leading order differential cross sections, and their matching to parton shower simulations*, *JHEP* **07** (2014) 079, [1405.0301].

[144] R. Frederix, S. Frixione, V. Hirschi, D. Pagani, H. S. Shao and M. Zaro, *The automation of next-to-leading order electroweak calculations*, *JHEP* **07** (2018) 185, [1804.10017].

[145] P. Nason, *A New method for combining NLO QCD with shower Monte Carlo algorithms*, *JHEP* **11** (2004) 040, [hep-ph/0409146].

[146] ATLAS Collaboration, *Studies of new Higgs boson interactions through nonresonant HH production in the $b\bar{b}\gamma\gamma$ final state in pp collisions at $\sqrt{s} = 13\,TeV$ with the ATLAS detector*, *JHEP* **01** (2024) 066, [2310.12301].

[147] CMS Collaboration, *Search for nonresonant Higgs boson pair production in final states with two bottom quarks and two photons in proton–proton collisions at $\sqrt{s} = 13\,TeV$*, *JHEP* **03** (2021) 257, [2011.12373].

[148] M. Cacciari and G. P. Salam, *Dispelling the N^3 myth for the k_t jet-finder*, *Phys. Lett. B* **641** (2006) 57–61, [hep-ph/0512210].

[149] M. Cacciari, G. P. Salam and G. Soyez, *The anti-k_t jet clustering algorithm*, *JHEP* **04** (2008) 063, [0802.1189].

[150] M. Cacciari, G. P. Salam and G. Soyez, *FastJet User Manual*, *Eur. Phys. J. C* **72** (2012) 1896, [1111.6097].

[151] ATLAS Collaboration, *Search for the non-resonant production of Higgs boson pairs via gluon fusion and vector-boson fusion in the $b\bar{b}\tau^+\tau^-$ final state in proton–proton collisions at $\sqrt{s} = 13\,TeV$ with the ATLAS detector*, *Phys. Rev. D* **110** (2024) 032012, [2404.12660].

[152] ATLAS collaboration, G. Aad et al., *Study of Higgs boson pair production in the $HH \to b\bar{b}\gamma\gamma$ final state with 308 fb^{-1} of data collected at $\sqrt{s} = 13\,TeV$ and 13.6 TeV by the ATLAS experiment*, 2507.03495.

[153] S. Frixione and B. R. Webber, *Matching NLO QCD computations and parton shower simulations*, *JHEP* **06** (2002) 029, [hep-ph/0204244].

[154] R. Frederix, S. Frixione, S. Prestel and P. Torrielli, *On the reduction of negative weights in MC@NLO-type matching procedures*, *JHEP* **07** (2020) 238, [2002.12716].

[155] X. Liu and F. Petriello, *Reducing theoretical uncertainties for exclusive Higgs-boson plus one-jet production at the LHC*, *Phys. Rev. D* **87** (2013) 094027, [1303.4405].

[156] I. W. Stewart, F. J. Tackmann, J. R. Walsh and S. Zuberi, *Jet p_T resummation in Higgs production at $NNLL' + NNLO$*, *Phys. Rev.* **D89** (2014) 054001, [1307.1808].

[157] R. Boughezal, X. Liu, F. Petriello, F. J. Tackmann and J. R. Walsh, *Combining Resummed Higgs Predictions Across Jet Bins*, *Phys. Rev. D* **89** (2014) 074044, [1312.4535].

[158] I. W. Stewart and F. J. Tackmann, *Theory Uncertainties for Higgs and Other Searches Using Jet Bins*, *Phys. Rev. D* **85** (2012) 034011, [1107.2117].

[159] S. Gangal and F. J. Tackmann, *Next-to-leading-order uncertainties in Higgs+2 jets from gluon fusion*, *Phys. Rev. D* **87** (2013) 093008, [1302.5437].

[160] ATLAS collaboration, G. Aad et al., *Measurement of the properties of Higgs boson production at $\sqrt{s} = 13$ TeV in the $H \to \gamma\gamma$ channel using 139 fb^{-1} of pp collision data with the ATLAS experiment*, *JHEP* **07** (2023) 088, [2207.00348].

[161] J. Bellm et al., *Herwig 7.0/Herwig++ 3.0 release note*, *Eur. Phys. J. C* **76** (2016) 196, [1512.01178].

[162] ATLAS collaboration, *Modelling of top-quark-mediated Higgs boson production in association with bottom quarks*, tech. rep., CERN, Geneva, 2025.

[163] E. Bagnaschi, F. Maltoni, A. Vicini and M. Zaro, *Lepton-pair production in association with a $b\bar{b}$ pair and the determination of the W boson mass*, *JHEP* **07** (2018) 101, [1803.04336].

[164] N. Moretti, P. Petrov, S. Pozzorini and M. Spannowsky, *Measuring the signal strength in $t\bar{t}h$ with $h \to b\bar{b}$*, *Phys. Rev. D* **93** (Jan, 2016) 014019.

[165] A. L. Kagan, G. Perez, F. Petriello, Y. Soreq, S. Stoynev and J. Zupan, *Exclusive Window onto Higgs Yukawa Couplings*, *Phys. Rev. Lett.* **114** (2015) 101802, [1406.1722].

[166] ATLAS collaboration, G. Aad et al., *Direct constraint on the Higgs-charm coupling from a search for Higgs boson decays into charm quarks with the ATLAS detector*, *Eur. Phys. J. C* **82** (2022) 717, [2201.11428].

[167] M. Cepeda et al., *Report from Working Group 2: Higgs Physics at the HL-LHC and HE-LHC*, *CERN Yellow Rep. Monogr.* **7** (2019) 221–584, [1902.00134].

[168] J. Baglio, C. Duhr, B. Mistlberger and R. Szafron, *Inclusive production cross sections at N^3LO*, *JHEP* **12** (2022) 066, [2209.06138].

[169] R. V. Harlander, S. Liebler and H. Mantler, *SusHi: A program for the calculation of Higgs production in gluon fusion and bottom-quark annihilation in the Standard Model and the MSSM*, *Comput. Phys. Commun.* **184** (2013) 1605–1617, [1212.3249].

[170] R. V. Harlander and W. B. Kilgore, *Higgs boson production in bottom quark fusion at next-to-next-to leading order*, *Phys.Rev.* **D68** (2003) 013001, [hep-ph/0304035].

[171] CMS collaboration, A. Hayrapetyan et al., *Observation of $WW\gamma$ production and search for $H\gamma$ production in proton-proton collisions at $\sqrt{s} = 13$ TeV*, *Phys. Rev. Lett.* **132** (2024) 121901, [2310.05164].

[172] CMS collaboration, V. Chekhovsky et al., *Search for γH production and constraints on the Yukawa couplings of light quarks to the Higgs boson*, 2502.05665.

[173] E. Balzani, R. Gröber and M. Vitti, *Light-quark Yukawa couplings from off-shell Higgs production*, *JHEP* **10** (2023) 027, [2304.09772].

[174] L. Alasfar, R. Gröber, C. Grojean, A. Paul and Z. Qian, *Machine learning the trilinear and light-quark Yukawa couplings from Higgs pair kinematic shapes*, *JHEP* **11** (2022) 045, [2207.04157].

[175] L. Alasfar, R. Corral Lopez and R. Gröber, *Probing Higgs couplings to light quarks via Higgs pair production*, *JHEP* **11** (2019) 088, [1909.05279].

[176] R. Gauld, *A massive variable flavour number scheme for the Drell-Yan process*, *SciPost Phys.* **12** (2022) 024, [2107.01226].

[177] M. Guzzi, P. Nadolsky, L. Reina, D. Wackeroth and K. Xie, *A general mass variable flavor number scheme for Z boson production in association with a heavy quark at hadron colliders*, 2410.03876.